Model-guided dynamic control of essential metabolic nodes boosts acetyl-coenzyme A–dependent bioproduction in rewired Pseudomonas putida

Kozaeva, Ekaterina; Volkova, Svetlana; Matos, Marta R.A.; Mezzina, Mariela P.; Wulff, Tune; Volke, Daniel C.; Nielsen, Lars K.; Nikel, Pablo I.

Published in:
Metabolic Engineering

Link to article, DOI:
10.1016/j.ymben.2021.07.014

Publication date:
2021

Document Version
Publisher's PDF, also known as Version of record

Metabolic Engineering 67 (2021) 373–386

Contents lists available at ScienceDirect

Metabolic Engineering

journal homepage: www.elsevier.com/locate/meteng

Model-guided dynamic control of essential metabolic nodes boosts acetyl-coenzyme A–dependent bioproduction in rewired *Pseudomonas putida*

Ekaterina Kozaeva [a], Svetlana Volkova [a], Marta R.A. Matos [a], Mariela P. Mezzina [a], Tune Wulff [a], Daniel C. Volke [a], Lars K. Nielsen [a,b], Pablo I. Nikel [a,*]

[a] The Novo Nordisk Foundation Center for Biosustainability, Technical University of Denmark, 2800, Kongens Lyngby, Denmark
[b] Australian Institute for Bioengineering and Nanotechnology (AIBN), The University of Queensland, Brisbane, QLD, 4072, Australia

ARTICLE INFO

Keywords:
Metabolic engineering
Synthetic biology
Pseudomonas putida
CRISPRi
Acetyl-CoA
Poly(3-hydroxybutyrate)

ABSTRACT

Pseudomonas putida is evolutionarily endowed with features relevant for bioproduction, especially under harsh operating conditions. The rich metabolic versatility of this species, however, comes at the price of limited formation of acetyl-coenzyme A (CoA) from sugar substrates. Since acetyl-CoA is a key metabolic precursor for a number of added-value products, in this work we deployed an *in silico*-guided rewiring program of central carbon metabolism for upgrading *P. putida* as a host for acetyl-CoA–dependent bioproduction. An updated kinetic model, integrating fluxomics and metabolomics datasets in addition to manually-curated information of enzyme mechanisms, identified targets that would lead to increased acetyl-CoA levels. Based on these predictions, a set of plasmids based on clustered regularly interspaced short palindromic repeats (CRISPR) and dead CRISPR-associated protein 9 (dCas9) was constructed to silence genes by CRISPR interference (CRISPRi). Dynamic reduction of gene expression of two key targets (*gltA*, encoding citrate synthase, and the essential *accA* gene, encoding subunit A of the acetyl-CoA carboxylase complex) mediated an 8-fold increase in the acetyl-CoA content of rewired *P. putida*. Poly(3-hydroxybutyrate) (PHB) was adopted as a proxy of acetyl-CoA availability, and two synthetic pathways were engineered for biopolymer accumulation. By including cell morphology as an extra target for the CRISPRi approach, fully rewired *P. putida* strains programmed for PHB accumulation had a 5-fold increase in PHB titers in bioreactor cultures using glucose. Thus, the strategy described herein allowed for rationally redirecting metabolic fluxes in *P. putida* from central metabolism towards product biosynthesis—especially relevant when deletion of essential pathways is not an option.

1. Introduction

After decades of continuous and intensive technological development, a broad range of bulk and fine chemicals, drugs and biofuels can be accessed by metabolic engineering of microorganisms (Choi et al., 2019; Ko et al., 2020; Nielsen and Keasling, 2016; Smanski et al., 2016). Multiple strategies have been deployed to this end, including the selection of suitable hosts for strain engineering (Becker and Wittmann, 2018; Calero and Nikel, 2019), modelling control of biochemical networks designed *in silico* (Fang et al., 2020; Volkova et al., 2020) and elimination or fine-tuned balancing of competing pathways (Nishida and Kondo, 2020; Shen et al., 2019)—an aspect supported by the ever expanding synthetic biology toolbox (Chen et al., 2020; Lammens et al., 2020; Young et al., 2021). In this sense, the inception of *Clustered Regularly Interspaced Short Palindromic Repeats* (CRISPR) and the *CRISPR-associated protein 9* (Cas9) of *Streptococcus pyogenes* played a central role in our ability to access and harness the metabolic potential of microbial species (Jakočiūnas et al., 2017; Tarasava et al., 2018; Zhao et al., 2021), including non-traditional bacterial platforms (Banerjee et al., 2020; Batianis et al., 2020; Kim et al., 2020; Tan et al., 2018; Weimer et al., 2020). Among the applications of CRISPR strategies relevant for metabolic engineering, repressing genes encoding key enzymes is very often required to balance metabolic pathways to increase production titers, yields and productivities (Schultenkämper et al., 2020). Hence, CRISPR elements have been repurposed for repressing gene expression (*CRISPR interference*, CRISPRi). This genetic tool only

* Corresponding author. The Novo Nordisk Foundation Center for Biosustainability, Technical University of Denmark, Lyngby, Denmark.
E-mail address: pabnik@biosustain.dtu.dk (P.I. Nikel).

https://doi.org/10.1016/j.ymben.2021.07.014
Received 31 May 2021; Received in revised form 23 July 2021; Accepted 29 July 2021
Available online 31 July 2021

requires an endonuclease activity-deficient version of Cas9, termed *dead Cas9* (dCas9), and a chimeric single-guide RNA (sgRNA) to recognize a DNA target of interest and block transcription of the cognate sequence (Larson et al., 2013; Zhang et al., 2021). CRISPRi is particularly useful for tuning metabolic or physiological traits encoded by essential genes, which precludes the implementation of gene deletions to eliminate the functions at stake (Domínguez et al., 2016; Gauttam et al., 2021; Xu and Qi, 2019).

Pseudomonas species sparked interest for a variety of metabolic engineering applications that require high levels of stress resistance and a versatile, resourceful metabolism (Akkaya et al., 2018; Bitzenhofer et al., 2021; Nikel and de Lorenzo, 2018). The model strain *P. putida* KT2440 has been used as a platform for production of bulk and fine chemicals (Banerjee et al., 2020; Bentley et al., 2020; Eng et al., 2021; Loeschcke and Thies, 2015; Volke et al., 2020a; Weimer et al., 2020), and this soil bacterium is also known as an efficient producer of biopolymers (Beckers et al., 2016; Mezzina et al., 2021; Prieto et al., 2016; Salvachúa et al., 2020)—especially medium-chain-length polyhydroxyalkanoates (PHAs). The metabolic versatility of *P. putida*, characterized by multiple catabolic modules that enable the use of multiple carbon and nitrogen sources (Poblete-Castro et al., 2020), comes at the price of a relatively low assimilation and biosynthetic efficiency (Belda et al., 2016; Sudarsan et al., 2014). A caveat hampering the broad adoption of *P. putida* as a bioproduction platform is a limited acetyl-coenzyme A (CoA) availability (Chohnan et al., 1997; Gläser et al., 2020), a key building block for added-value compounds, e.g. fatty acids, PHAs, isoprenoids, sterols and alcohols (Barajas et al., 2017; Kiefer et al., 2021). The evolutionary adoption of the Entner-Doudoroff (ED) pathway as the main catabolic module for sugars, and part of the EDEMP cycle (Chavarría et al., 2013; Nikel et al., 2015), is the main reason behind this occurrence. As recently demonstrated by Sánchez-Pascuala et al. (2019), the functional replacement of the native catabolism by a synthetic Embden-Meyerhof-Parnas glycolysis increased the acetyl-CoA pool—but the engineered *P. putida* strain grew slowly and only reached moderate cell densities. Hence, balancing the acetyl-CoA node, a metabolic hub where multiple reactions (several of which are essential) converge and branch out, requires a delicate fine-tuning of fluxes (Ku et al., 2020).

On the background exposed above, in this work we built and interrogated a core kinetic model of *P. putida* KT2440 central carbon metabolism to identify key targets for manipulation towards increasing acetyl-CoA availability. Essential metabolic functions emerged as the main sink for the thioester, and we deployed a CRISPRi system for redirecting metabolic fluxes towards acetyl-CoA by depleting substrate-competing proteins. The effectiveness of this dynamic regulation approach was demonstrated by metabolomic and proteomic analyses in engineered strains where the fluxes around the acetyl-CoA node have been downregulated by direct interference of essential metabolic functions. The utility of dynamic metabolic regulation was further illustrated by implementing two synthetic routes for poly(3-hydroxybutyrate) (PHB) accumulation, the most widespread short-chain-length PHA with applications in medicine, agriculture and food industry (Choi et al., 2020). PHB biosynthesis exclusively relies on acetyl-CoA as the precursor (Anderson and Dawes, 1990), and it can be used as a proxy of the intracellular availability of this coenzyme. The multi-level CRISPRi approach not only enabled a substantial redirection of fluxes towards product synthesis, but this strategy also improved PHB accumulation by manipulating the cell morphology in fully automated bioreactor cultures.

2. Materials and methods

2.1. Bacterial strains, plasmids and culture conditions

Bacterial strains and plasmids used in this study are listed in Table 1. *Escherichia coli* and *P. putida* cultures were incubated at 37 °C and 30 °C,

Table 1
Bacterial strains and plasmids used in this study.

Bacterial strain	Relevant characteristics[a]	Reference or source
Escherichia coli		
DH5α λ*pir*	Cloning host; F^- λ^- *endA1 glnX44*(AS) *thiE1 recA1 relA1 spoT1 gyrA96*(Nal^R) *rfbC1 deoR nupG* Φ80(*lacZ*Δ*M15*) Δ(*argF-lac*)*U169 hsdR17*(r_K^- m_K^+), λ*pir* lysogen	Hanahan and Meselson (1983)
Pseudomonas putida		
KT2440	Wild-type strain, derived from *P. putida* mt-2 (Worsey and Williams, 1975) cured of the catabolic TOL plasmid pWW0	Bagdasarian et al. (1981)
EM42	Reduced-genome derivative of strain KT2440; Δprophage1 Δprophage4 Δprophage3 Δprophage2 ΔTn*7* Δ*endA*-1 Δ*endA*-2 Δ*hsdRMS* Δflagellum ΔTn*4652*	Martínez-García et al. (2014b)
SEM1.3	Reduced-genome derivative of strain EM42; Δ*phaC1ZC2DFI* (Δ*PP_5003-PP_5008*) Δ*benABCD* (Δ*PP_3161-PP_3164*)	This work
Plasmid	**Relevant characteristics[a]**	**Reference or source**
pMCRi	Plasmid for CRISPRi; *oriV* (pRO1600/ColE1), *xylS* (cured of *Bsa*I-sites), *Pm→dCas9*^{Sp}, P_{EM7}→sgRNA; Sm^R/Sp^R	Batianis et al. (2020)
pMCRi_*gltA*	Plasmid for CRISPRi; *oriV* (pRO1600/ColE1), *xylS* (cured of *Bsa*I-sites), *Pm→dCas9*^{Sp}, P_{EM7}→*gltA*-specific sgRNA; Sm^R/Sp^R	This work
pMCRi_*accA*	Plasmid for CRISPRi; *oriV* (pRO1600/ColE1), *xylS* (cured of *Bsa*I-sites), *Pm→dCas9*^{Sp}, P_{EM7}→*accA*-specific sgRNA; Sm^R/Sp^R	This work
pMCRi_*accC*	Plasmid for CRISPRi; *oriV* (pRO1600/ColE1), *xylS* (cured of *Bsa*I-sites), *Pm→dCas9*^{Sp}, P_{EM7}→*accC*-specific sgRNA; Sm^R/Sp^R	This work
pMCRi_*ftsZ*	Plasmid for CRISPRi; *oriV* (pRO1600/ColE1), *xylS* (cured of *Bsa*I-sites), *Pm→dCas9*^{Sp}, P_{EM7}→*ftsZ*-specific sgRNA; Sm^R/Sp^R	Batianis et al. (2020)
pMCRi_*gltA_accA*	Plasmid for dual CRISPRi; *oriV* (pRO1600/ColE1), *xylS* (cured of *Bsa*I-sites), *Pm→dCas9*^{Sp}, P_{EM7}→*gltA*- and *accA*-specific sgRNAs; Sm^R/Sp^R	This work
pMCRi_*gltA_accA_ftsZ*	Plasmid for triple CRISPRi; *oriV* (pRO1600/ColE1), *xylS* (cured of *Bsa*I-sites), *Pm→dCas9*^{Sp}, P_{EM7}→*gltA*-, *accA*- and *ftsZ*-specific sgRNAs; Sm^R/Sp^R	This work
pGNW2	Suicide vector used for deletions in Gram-negative bacteria; *oriT*, *traJ*, *lacZα*, *ori*(R6K), P_{EM7}→*msfGFP*; Km^R	Wirth et al. (2020)
pGNW2·Δ*ben*A-D	Derivative of vector pGNW2 carrying homology regions to delete *benABCD* (*PP_3161-PP_3164*); Km^R	Volke et al. (2020b)
pGNW2·Δ*phaC-I*	Derivative of vector pGNW2 carrying homology regions to delete *phaC1ZC2DFI* (*PP_5003-PP_5008*); Km^R	This work
pSEVA2311	Expression vector; *oriV*(pBBR1), *chnR*, P_{chnB} (standardized, cyclohexanone-responsive expression system); Km^R	Benedetti et al. (2016); Silva-Rocha et al. (2013)

(*continued on next page*)

Table 1 (*continued*)

Bacterial strain	Relevant characteristics[a]	Reference or source
pS2311·PHA	Derivative of vector pSEVA2311; canonical PHB biosynthesis route; P_{chnB}→*phaCAB* from *Cupriavidus necator*, including synthetic RBSs in front of each gene	This work
pS2311·PHAS	Derivative of vector pSEVA2311; alternative, NphT7-dependent PHB biosynthesis route; P_{chnB}→*nphT7 phaCB*; *phaCB* from *C. necator* and *nphT7* from *Streptomyces* sp. strain CL190, including synthetic RBSs in front of each gene	This work

[a] Antibiotic markers: Km, kanamycin; Nal, nalidixic acid; Sm, streptomycin; and Sp, spectinomycin.

respectively. For cloning procedures and during genome engineering manipulations, cells were grown in lysogeny broth (LB) medium (10 g L^{-1} tryptone, 5 g L^{-1} yeast extract and 10 g L^{-1} NaCl; solid culture media additionally contained 15 g L^{-1} agar). All shaken-flask cultures were agitated at 200 rpm (MaxQ™ 8000 incubator; ThermoFisher Scientific, Waltham, MA, USA). Kanamycin (Km), gentamicin (Gm) and streptomycin (Str) were added whenever needed at 50 μg mL^{-1}, 10 μg mL^{-1} and 100 μg mL^{-1}, respectively. Unless otherwise indicated, shaken-flask and automated bioreactor cultures were conducted in de Bont minimal medium [Table S1 in the Supplementary Data, formulated according to Hartmans et al. (1989)] containing 1% (w/v) glucose as the carbon source. The optical density measured at 600 nm (OD_{600}) was recorded in a Genesys 20 spectrophotometer (Thermo Fisher Scientific) to estimate bacterial growth. During physiological characterization of engineered strains, growth kinetics were followed at OD_{600} with light path correction in a Synergy™ MX microtiter plate reader (BioTek Instruments Inc., Winooski, VT, USA).

2.2. General cloning procedures and construction of plasmids and mutant strains

All plasmids and oligonucleotides used in this work are listed in Table 1 and Table S2 in the Supplementary Data, respectively. Unless stated otherwise, uracil-excision (*USER*) cloning (Cavaleiro et al., 2015) was used for the construction of all plasmids. The *AMUSER* tool was employed for designing oligonucleotides (Genee et al., 2015); Phusion™ *U* high-fidelity DNA polymerase (ThermoFisher Scientific) was used according to the manufacturer's specifications in amplifications intended for *USER* cloning. For colony PCR, the commercial *OneTaq*™ master mix (New England BioLabs, Ipswich, MA, USA) was used according to the supplier's instructions. *E. coli* DH5α λ*pir* (Table 1) was employed as a host for general cloning purposes. Chemically-competent *E. coli* cells were prepared and transformed with plasmids using the *Mix and Go*™ commercial kit (Zymo Research, Irvin, CA, USA) according to the manufacturer's indications. Electrocompetent *P. putida* cells were prepared by washing the biomass from LB medium cultures with 300 mM sucrose, followed by transformation with plasmids by electroporation (Choi et al., 2006; Volke et al., 2020c). Gene deletions were implemented by antibiotic-free allelic exchange assisted by curable plasmids (Volke et al., 2020b; Wirth et al., 2020). The sequence of all plasmids and strains was verified by Mix2Seq sequencing (Eurofins Genomics, Ebersberg, Germany).

2.3. Ensemble model building

The General Reaction Assembly and Sampling Platform (*GRASP*) developed by Saa and Nielsen (2015) was used to build and parametrize a thermodynamically consistent kinetic model of central carbon metabolism for *P. putida* KT2440. In this framework, each reaction is decomposed into elementary reactions according to its enzyme mechanism (Cleland, 1963), which specifies the order of substrate binding and product release. Each elementary reaction was modeled using mass action kinetics. Following the ensemble modelling framework (Tran et al., 2008), *GRASP* calculates the rate constant values as a function of (i) the change in the Gibbs free energy ($\Delta_r G'$) of the reaction, (ii) reference reaction fluxes and (iii) reference metabolite concentrations. We started by listing all the reactions in the biochemical network of *P. putida* KT2440 representing central carbon metabolism (Tables S3 and S4 in the Supplementary Data). To parameterize the models within the *GRASP* framework, we resorted to: (i) a reference flux distribution from glucose-grown *P. putida* KT2440 (Nikel et al., 2015, 2021); (ii) steady-state metabolite concentrations in mol L^{-1} and $\Delta_r G'^0$ values from *eQuilibrator* (Flamholz et al., 2012) to calculate $\Delta_r G'$ for each reaction; (iii) enzyme mechanisms, including order of binding and release of reactants, number of subunits for each enzyme, and (iv) information on enzyme regulation, i.e. any known allosteric effectors as well as inhibitors or activators (all this information is listed in Table S4-S9 in the Supplementary Data). In this way, an ensemble of kinetic models was built where each model reaches the reference state and is consistent with experimental data and additional information about the system. The ensemble is composed by 10,000 independent models and was used to perform *metabolic control analysis* (MCA) (Moreno-Sánchez et al., 2008) in order to find which enzymes can affect the steady-state acetyl-CoA concentration. A detailed explanation on model building and validation is presented in Supplementary Methods S1.

2.4. LC-MS–assisted metabolomic analysis

At the indicated time-points, 1-mL culture aliquots were withdrawn and the biomass was harvested by vacuum filtering (Durapore™ Membrane Filter, 0.45 μm). Upon filtration, cells were quenched with 3 mL of an acetonitrile–CH_3OH–water solution [40-40-20% (v/v)] and acidified with 0.1 M formic acid at −20 °C (Rabinowitz and Kimball, 2007). Subsequently, cell debris were removed by centrifugation at 17,000×*g* for 10 min as described in Nikel et al. (2021). The supernatant was transferred to a new tube and solvents were removed by evaporation at 30 °C for 90 min at reduced pressure (Concentrator Plus, Eppendorf, Hamburg, Germany). The samples were freeze dried and stored at −80 °C. Prior to analysis, the sediment was reconstituted in 100 μL of deionized water and insoluble particles were removed by centrifugation at 17,000×*g* for 10 min. Metabolites were quantified using LC-MS/MS according to the method of McCloskey et al. (2016), and the chromatograms were analyzed using the MultiQuant™ software (Sciex, CA, USA). The Prism 8 software (GraphPad Software Inc., San Diego, CA, USA) was used to plot results obtained for selected metabolites. The Matplotlib (NumPy based cross-platform) library was used in order to visualize data as heatmap (Hunter, 2007). The mean metabolite concentrations across replicates were taken and normalized to the mean value of the control condition for this analysis.

2.5. Genome-wide targeted proteomics analysis by LC-MS/MS

A genome-wide proteomics analysis was used to quantify relative levels of pathway proteins in samples from 50-mL shaken-flask cultures. At the time points indicated in the text, 1-mL aliquots from each culture were pelleted at 10,000×*g* for 10 min and flash-frozen with liquid nitrogen. Pellets were stored at −80 °C until they were processed according to the procedure of Bongers et al. (2020). Cells were lysed in 6 M guanidinium·HCl, 5 mM *tris*(2-carboxyethyl)phosphine, 10 mM chloroacetamide and 100 mM Tris·HCl (pH = 8.5) while being disrupted in a Mixer Mill (MM 400 Retsch, Haan, Germany) set at 25 Hz for 5 min at room temperature, followed by 10 min in a thermomixer at 95 °C at 2,

000 rpm. A clarified supernatant was obtained by centrifugation at 15,000×*g* for 10 min. The protein concentration in the cell-free lysate was estimated by means of the bicinchoninic acid method, and 100 μg of proteins were tryptically digested for 8 h. After this digestion step, 10 μL of 10% (w/v) trifluoroacetic acid was added and samples were fractionated using a StageTip C18 (Empore, 3M, USA). Next, 1 μg of the purified peptides was injected into an Orbitrap Exploris 480 mass spectrometer (Thermo Scientific). The instrument was operated in data dependent acquisition mode, and the listed settings MS-level scans were performed with Orbitrap resolution set at 120,000; AGC target of 300%; maximum injection time set in auto; intensity threshold at 5.0×10^3 and dynamic exclusion of 20 s. Data-dependent MS2 selection was performed in Top 20 Speed mode with HCD collision energy set to 40% (AGC target = 75, maximum injection time of 30 ms and isolation window of 1.3 *m/z*). The peptides were eluted over a gradient from 4% (v/v) acetonitrile in water to 76% (v/v) over a total of 60 min. The raw files were analyzed in the Proteome discoverer 2.4 software with the following settings: fixed modifications, carbamidomethyl and variable modifications, and oxidation of methionine residues. The first search was set to a mass tolerance of 20 ppm and a MS/MS tolerance of 20 ppm, trypsin as an enzyme and allowing one missed cleavage. The false discovery rate was set at 0.1%, and the match-between-runs window was defined as 0.7 min. Quantifications were performed including only unique peptides and normalization between samples was based on total peptide amounts. A protein database, consisting of the *P. putida* reference proteome (UP000000556) together with the amino acid sequence of the heterologous proteins (when relevant), was used for sequence identification. Bioinformatic analysis was performed in Python, and a principal component analysis (PCA) was firstly run for quality control purposes. PCA was done *via* sklearn.decomposition.PCA to perform dimensional reduction using standardized data. Two-sample Student's *t*-test was used to determine which proteins displayed significantly changed abundance between control and experimental groups with a false discovery rate of 0.01% corrected by the Benjamini-Hochberg method (Ferreira, 2007). For this purpose, scipy.stats.ttest_ind was used to calculate *t*-test probabilities for the means of two independent samples. Enzymes involved in reactions within the central carbon metabolism of *P. putida* KT2440 were identified by the gene-protein-reaction rule by using the genome-scale metabolic model *i*JN1463 (Nogales et al., 2020). The same set of reactions of central carbon metabolism was chosen as per the kinetic model. Matplotlib library was used to visualize data as heatmap as explained above. The mean values across replicates were taken and normalized to the mean value of control conditions across experiments. In both metabolomics and proteomic analyses, the lowest value for the color scheme of a heatmap is 0.1 and the biggest is 2.5, which means that any value smaller than 0.1 or bigger than 2.5 is visualized with the same color as for 0.1 or 2.5, respectively. Metabolic pathway enrichment analysis was performed in order to determine metabolic pathways with enriched proteins with altered abundance. Protein sets with significantly increased and decreased abundance in every comparison group were used to run the analysis. The Biocyc online resource (Karp et al., 2015) and the associated SmartTables facility (https://biocyc.org/smarttables) were chosen for this analysis. The pathways were selected for *P. putida* and a *P*-value of 0.05 was set as a threshold for significance. Gene ontology analysis was furthermore used to establish a hierarchy of pathways enriched in proteins that showed either increased or decreased abundance across experimental conditions. The full set of proteins in these classifications is listed in Tables S10–S15 in the Supplementary Data, with a detailed graphical representation of this ontology analysis shown in Figs. S4–S6.

2.6. Analysis of PHB by methanolysis and GC-FID detection of methyl esters

This method was adapted from the protocol originally reported by Braunegg et al. (1978) and modified by Ruiz et al. (2006). In order to optimize reaction conditions, samples (either pure PHB or biomass) were firstly dissolved in 2 mL of CH_3OH with four concentrations [1%, 3%, 5% or 15% (v/v)] of H_2SO_4 and 2 mL of $CHCl_3$ in a screw-capped, Teflon-stoppered test tube. The solution was then incubated at 100 °C for 4–6 h. After cooling to room temperature, 1 mL of a 1 M NaCl solution or water was added to the tubes, and the samples were shaken for 10 min. The two phases were separated by leaving the tubes at room temperature for 6 h without shaking. The organic phase was collected in a new test tube and dried over 15 mg of anhydrous Na_2SO_4 prior to GC analysis, and benzoate (0.5 mg mL^{-1}) was included as internal standard compound in separate measurements. In the case of samples from bioreactor fermentations, the biomass was pelleted *via* centrifugation (17,000×*g* for 10 min) and lyophilized in a freeze drier for 24 h. For methanolysis, 5–10 mg of the dried biomass was treated with 2 mL of CH_3OH containing 15% (v/v) of H_2SO_4 and 2 mL of $CHCl_3$, with benzoate as internal standard. The suspension was incubated at 100 °C for 4 h and, after cooling to room temperature, 1 mL of water was added to each sample, mixed and centrifuged at 4000×*g* for 15 min to accelerate phase separation. The aqueous phase was discarded, and samples were additionally washed with 1 mL of water to remove any H_2SO_4 traces. After drying over Na_2SO_4, the organic phase was then used for gas chromatography–flame ionization detection (GC-FID) analysis. These optimized conditions for extraction and methanolysis were kept for further experiments as they yielded consistent results across standards and experimental samples. A GC column BPX-5 (BGB Analytik, Rheinfelden, Germany; 30 m × 0.3 mm × 0.1 μm) was used to separate the esterified monomers at 275 °C as indicated elsewhere (Martínez-García et al., 2014a; Nikel et al., 2006). Absolute amounts of PHB were determined by means of both the internal and the PHB standard, and expressed either as a concentration or as a percentage referred to the cell dry weight (CDW). A detailed explanation on how these values were calculated is provided in the Supplementary Data. Direct visualization of intracellular PHB granules was carried out by fluorescence microscopy after staining the cells with a 0.5 μg mL^{-1} Nile Red solution in dimethyl sulfoxide (Spiekermann et al., 1999). Procedures for light field microscopy were done as described by Batianis et al. (2020), and fluorescence microscopy pictures were taken with a filter for Nile Red detection (excitation wavelength = 549 nm and emission wavelength = 628 nm).

2.7. Cultivation of P. putida strains in automated multi-parallel bioreactors

Batch bioreactor experiments were carried out in a 12-way Ambr™ 250 bioreactor system equipped with single-use, disposable bioreactors (microbial vessel type) in a fully automated platform (Sartorius Lab Instruments GmbH & Co. KG, Goettingen, Germany). The vessels were filled with 150-mL de Bont minimal media containing 1% (w/v) glucose as the carbon source. The temperature was maintained at 30 °C throughout the fermentation process and the agitation was set constant to 1300 rpm. Airflow was kept at 1 vessel volume min^{-1} during the entire run and the pH was maintained at 7.0 by automatic addition of 2 N NaOH. All bioreactors were inoculated manually with 5 mL of a shaken-flask pre-culture with the same medium composition. Pre-cultures were harvested in exponential phase, and the initial OD_{600} of each bioreactor culture was normalized. Whenever needed, bioreactor cultures were added with cyclohexanone and 3-methylbenzoate (3-*m*Bz) at 1 mM as chemical inducers of the ChnR/P_{chnB} and XylS/*Pm* expression systems, respectively, at 5 h post-inoculation. Samples were taken at the times indicated in the text for analytical determinations. The built-in Ambr™ 250 RunTime software and a fully automated liquid handler was used to execute all process steps.

2.8. Data and statistical analysis

All the experiments reported were independently repeated at least

three times (as indicated in the corresponding figure or table legend), and the mean value of the corresponding parameter ± standard deviation is presented. When relevant, the level of significance of differences when comparing results was evaluated by ANOVA (Barlett's test, Prism 8, GraphPad software, San Diego, CA, USA) with a P value = 0.01, as indicated in the figure legends. *GRASP* was encoded and implemented in MATLAB™; the analysis was performed in Matlab R2018a. To compute feasible ranges of Gibbs free energy, the Gurobi Optimizer version 9.0.3 (build v9.0.3rc0) was used with the following parameters: optimality tolerance = 1×10^{-6}; feasibility tolerance = 1×10^{-6}; and integer feasibility tolerance = 1×10^{-5}. Each model was checked for linear stability using a threshold of the Jacobian's eigenvalues of 1×10^{-5}. For MCA, a step size of 1×10^{-10} was used. All data and code used in omic data analysis and kinetic model construction is freely available in GitHub (https://github.com/svevol/accoa_project_data_analysis).

3. Results and discussion

3.1. Metabolic control analysis using a core kinetic model of P. putida KT2440 reveals key targets for manipulation towards increasing acetyl-CoA availability

Acetyl-CoA, a key intermediate in central carbon metabolism and essential building block for the majority of industrially-relevant compounds, is highly interconnected to other metabolic nodes. We first explored which interventions hold most potential to increase acetyl-CoA availability in *P. putida* KT2440. To this end, we used *GRASP* (Saa and Nielsen, 2015) to build an ensemble of kinetic models representing the biochemical network of *P. putida* KT2440. The model proposed herein is focused on the reactions of central carbon metabolism, including comprehensive kinetic mechanisms. Building on the latest genome-scale metabolic reconstructions for strain KT2440 (Belda et al., 2016; Nogales et al., 2020), our core kinetic model comprising a detailed description of the reactions involved in glucose uptake (and oxidized derivatives of the sugar), glycolysis (embodied by the EDEMP cycle), pentose phosphate pathway and tricarboxylic acid (TCA) cycle (Fig. 1A and Table S3 in the Supplementary Data). In addition, the model includes (i) three key reactions for fatty acid biosynthesis, which directly consume acetyl-CoA as the precursor or use this coenzyme as acyl donor (coded as ACCOAC, MCOATA and KAS15), (ii) two lumped reactions for oxidative phosphorylation (either NADH- or quinone-dependent) and (iii) five reactions for cofactor regeneration that ensure that their intracellular concentrations are balanced under (pseudo) steady-state conditions. In particular, ACCOAC represents the reaction of acetyl-CoA carboxylase, which provides malonyl-CoA as the key starter of fatty acid synthesis. MCOATA and KAS15 are reactions catalyzed by FabB [malonyl-CoA-–acyl carrier protein (ACP) transacylase] and the FabH condensing enzyme, respectively. These reactions initiate the cycles of fatty acid elongation by condensing acyl-CoA primers with malonyl-ACP (Mezzina et al., 2021; Thompson et al., 2020). Furthermore, and in order to increase the accuracy of the *in silico* predictions, the kinetic mechanism of 42 enzymes of central carbon metabolism in strain KT2440 was included in the reconstruction (Tables S4 and S5 in the Supplementary Data). Moreover, the known regulatory patterns (e.g. allosteric inhibition or

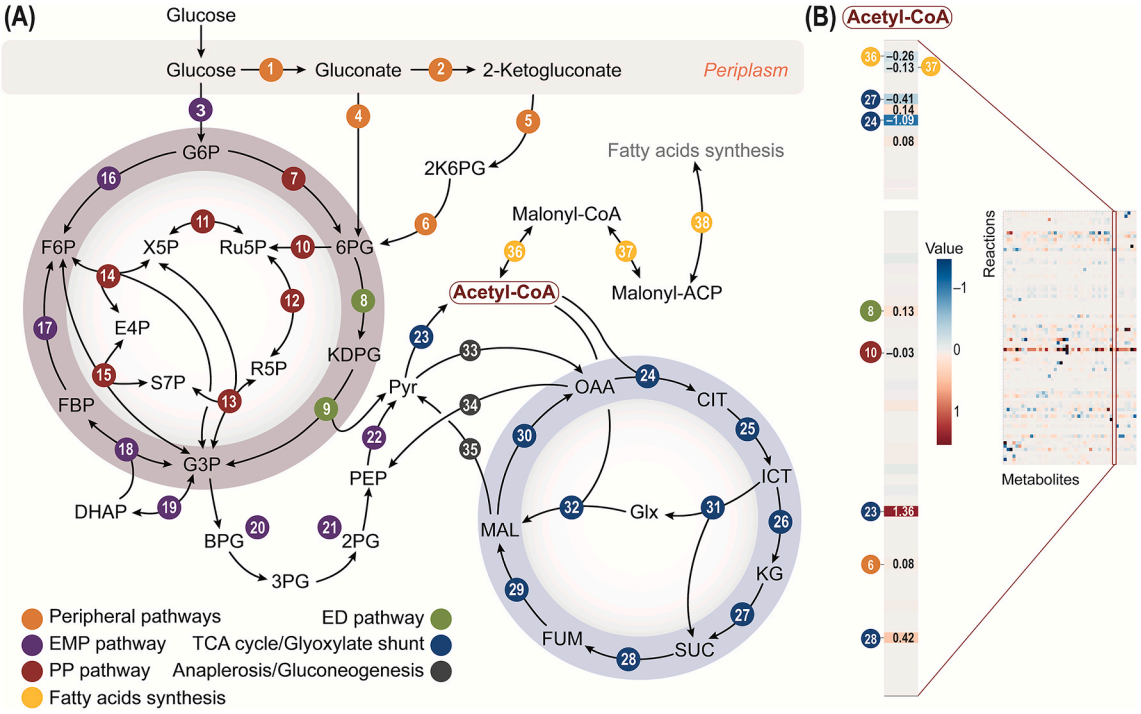

Fig. 1. ***In silico*** **analysis of metabolic nodes to increase acetyl-CoA availability in** ***P. putida*****. (A)** Biochemical network used to build the core kinetic model of *P. putida* KT2440 towards altering acetyl-CoA availability. The model includes the following modules: Embden-Meyerhof-Parnas (EMP) pathway, Entner-Doudoroff (ED) pathway, pentose phosphate (PP) pathway, tricarboxylic acids (TCA) cycle, as well as the glucose, gluconate and 2-ketogluconate uptake routes and gluconeogenesis (Nikel et al., 2015, 2021). In addition, the kinetic reconstruction includes (i) fatty acid synthesis from malonyl-coenzyme A (CoA) (v_{38}), (ii) reactions involved in cofactor regeneration and (iii) two lumped reactions to model oxidative phosphorylation. The full list of reactions is provided in the Supplementary Data. Abbreviations for the metabolites in the network are as follows: G6P, glucose-6-P; F6P, fructose-6-P; FBP, fructose-1,6-P_2; DHAP, dihydroxyacetone-P; 6PG, 6-phosphogluconate; KDPG, 2-keto-3-deoxy-6-phosphogluconate; Ru5P, ribulose-5-P; R5P, ribose-5-P; X5P, xylulose-5-P; S7P, sedoheptulose-7-P; E4P, erythrose-4-P; G3P, glyceraldehyde-3-P; 3PG, glycerate-3-P; PEP, phosphoenolpyruvate; Pyr, pyruvate; Acetyl-CoA, acetyl-coenzyme A; Malonyl-CoA, malonyl-coenzyme A; OAA, oxaloacetate; CIT, citrate; ICT, isocitrate; KG, 2-ketoglutarate; SUC, succinate, FUM, fumarate; MAL, malate and Glx, glyoxylate. **(B)** Heatmap representing concentration control coefficient (CCC) values for acetyl-CoA for each reaction in the model, identified with the same code number as in **(A)**. In total, 78 reactions and 45 metabolites were accounted for in the model. The detailed heatmap and the full list of all computed CCC values in the biochemical network is provided in Fig. S2 in the Supplementary Data.

activation) for key enzymes [i.e., Zwf (glucose-6-P dehydrogenase), GntZ (6-phosphogluconate dehydrogenase), Edd (6-phosphogluconate dehydratase), Pyk (pyruvate kinase), the malic enzyme, isocitrate dehydrogenase and citrate synthase] were likewise added to the core model (Table S6). In order to find the steady-state distribution of the fluxes given the set of reactions included, the *i*JN1463 reconstruction (Nogales et al., 2020) was analyzed by means of parsimonious enzyme usage flux balance analysis (pFBA) (Lewis et al., 2010) with glucose as the carbon source. The model was constrained with the flux values obtained in glucose-grown *P. putida* KT2440 (Nikel et al., 2015). A consistency check was firstly implemented to validate the model (Fig. S1) by evaluating *in silico* metabolic knock-outs (glucose transporter), knock-downs (Edd) and metabolic perturbations (ATP and NADPH deficiency). The results of these simulations showed a promising predictive power towards the metabolism of *P. putida* as reflected, for instance, in the projected time-resolved profile of normalized ATP, NADPH, acetyl-CoA and pyruvate concentrations (Fig. S1), which followed previously reported experimental observations (Nikel et al., 2021). With this validated kinetic model at hand, we ran metabolic control analysis (MCA) to identify reactions that affect acetyl-CoA availability (Fig. 1B and Fig. S2 in the Supplementary Data) in the form of concentration control coefficients (CCC) for acetyl-CoA, thereby guiding the process of target evaluation.

Despite the high degree of interconnectivity of the acetyl-CoA node, only a few biochemical reactions were found to be responsible for significant changes of the steady-state concentration of the coenzyme. As indicated in Fig. 1B, the reactions with the highest CCC absolute values were PDH (v_{23}, the pyruvate dehydrogenase complex, 1.36), AKGDH (v_{27}, α-ketoglutarate dehydrogenase, −0.41), CS (v_{24}, citrate synthase, −1.09), ACCOAC (v_{36}, acetyl-CoA carboxylase—one of the reactions explicitly added to the updated model, −0.26) and SUCDi (v_{28}, component of succinate dehydrogenase, 0.42). PDH is the only reaction in the model that produces acetyl-CoA, thus it had a high positive impact on the coenzyme concentration at steady-state; i.e., the higher the flux through PDH, the higher the acetyl-CoA availability. Out of the several reactions that depleted acetyl-CoA, CS and ACCOAC had the most significant impact on the simulated coenzyme concentration. CS seemed to have a larger effect as compared to ACCOAC, which is likely due to the significantly higher flux through the former reaction over that of ACCOAC (Nikel et al., 2015). Since malonyl-CoA is only needed at relatively low levels for lipid biosynthesis (Polyak et al., 2012), the ACCOAC flux through it is comparatively low. AKGDH, part of the TCA cycle, had a moderately negative impact on acetyl-CoA concentration as it consumes CoA, thus competing with PDH and impacting acetyl-CoA production. Interestingly, SUCDi showed a positive effect on the coenzyme availability, as a higher flux through SUCDi would redirect the carbon flow from the TCA cycle into gluconeogenesis (i.e., using the malic enzyme instead of malate dehydrogenase), which then leads to a higher flux through PDH by replenishing the pyruvate pool. Increasing the PDH flux by direct manipulation of the cognate genes, however, has proven very difficult due to the intricate regulatory patterns of this enzymatic complex (Ku et al., 2020), and we discarded this possibility. SUCDi, on the other hand, is a membrane complex, and overexpressing the cognate genes would be likewise tricky, potentially leading to protein aggregation. Therefore, the pFBA and CCC analyses pointed to two obvious metabolic targets for downregulation: CS (encoded by *gltA*, *PP_4194*) and ACCOAC (Acc, a complex with four subunits encoded by *accA*, *PP_1607*, *accB*, *PP_0559*, *accC*, *PP_0558* and *accD*, *PP_1996*). Both reactions are considered essential for survival in bacteria (Tokuyama et al., 2019; Tovilla-Coutiño et al., 2020; Udaondo et al., 2016), and their elimination by gene knockouts is therefore not an option—which makes them attractive targets for CRISPRi-mediated transcriptional tuning of the cognate genes, as explained in the next section.

3.2. Single and dual CRISPRi-mediated knock-down balances acetyl-CoA levels in reduced-genome *P. putida* strains

We developed a series of 3-*m*Bz–inducible CRISPRi plasmids (pMCRi) for tuning gene expression of single and multiple gene targets in *P. putida* (Fig. 2A). The direct cloning of spacers against different genes in vector pMCRi is facilitated by the introduction of *Bsa*I restriction sites, and the *dCas9* gene from *Streptococcus pyogenes* in this plasmid is placed under transcriptional control of the XylS/*Pm* expression system. In parallel, *P. putida* EM42, a reduced-genome derivative of strain KT2440 (Martínez-García et al., 2014b), was further refactored to facilitate the use of our CRISPRi toolbox towards establishing a platform strain for acetyl-CoA–dependent bioproduction. As *P. putida* metabolizes benzoates (Feist and Hegeman, 1969; Jiménez et al., 2002), resulting in the formation of brown-colored products [catechols and polymers thereof; Jiménez et al. (2014)], the *benABCD* cluster was deleted in strain EM42 to abolish oxidation of 3-*m*Bz. This operation rendered 3-*m*Bz a gratuitous inducer of the XylS/*Pm* system and allowed for precise OD_{600} measurements in the cultures without the interference typically caused by catechols and polymerization products. Additionally, since PHB biosynthesis was selected as a proxy of the intracellular acetyl-CoA availability, we removed the endogenous *pha* gene cluster, comprising *phaC1ZC2DFI*, to avoid any potential cross-talk between the synthetic PHB biosynthesis routes (described in the next section) and the native machinery for medium-chain-length PHAs formation, including regulatory and granule-associated proteins (Mezzina et al., 2021). This derivative of *P. putida* EM42, termed *P. putida* SEM1.3 (Table 1), was constructed by I-*Sce*I–mediated recombination (Wirth et al., 2020) and was used as a host in the experiments described below.

A set of pMCRi-derivative plasmids was constructed by cloning synthetic spacers against *gltA* (encodes CS), *accA* and *accC* (encoding the A and C subunits of the ACCOAC complex) or a combination of them (Fig. 2A). We focused on the first and the last reaction catalyzed by the ACCOAC complex, where AccA (carboxyltransferase) and AccC play a key role. The *accC* gene (encoding biotin carboxylase) forms an operon with *accB* (encoding a biotin carboxyl carrier protein), and blocking each gene individually would probably have a similar effect on the overall stoichiometry (hence, the activity) of the ACCOAC complex as shown in *E. coli* (Smith and Cronan, 2012). The resulting plasmids were transferred to *P. putida* SEM1.3 (Table 1), and the growth profile of the recombinant strains was determined in de Bont minimal medium containing glucose as the carbon source in microtiter plate cultures (Fig. 2B). All strains harboring pMCRi plasmids with sgRNAs against *gltA*, *accA* or *accC* had a slower growth and achieved lower biomass densities by the end of the experiment than *P. putida* SEM1.3 transformed with the control vector. The strongest effect on growth was seen for *P. putida* SEM1.3 with CRISPRi-mediated repression of *gltA* and *accA*. In these two cases, the specific growth rate (μ) was reduced by ca. 40% and 20%, respectively, with a final biomass density of ca. 80% of that in control cultures. Repressing *accC* expression, in contrast, had a negligible effect on the cell density—hence, this target was discarded in further CRISPRi experiments. The two most efficient sgRNAs were combined to build plasmid pMCRi_*gltA*_*accA* for dual target repression (Fig. 2C). *P. putida* SEM1.3 carrying this plasmid had a reduction in μ values of ca. 30% in glucose cultures as compared to the control experiment, suggesting a synergistic (but not necessarily additive) effect of repressing the expression of *gltA* and *accA*. These *P. putida* strains, with a 'rewired' acetyl-CoA node by CRISPRi, were subjected to further analysis to unveil the metabolic determinants of the growth patterns observed. To this end, the metabolomic profile of rewired strains grown in shaken-flask cultures using glucose as the sole carbon source was monitored in a time-course LC-MS/MS experiment. The full metabolomic dataset, which includes 80 individual metabolites and cofactors within the core reactions of central carbon metabolism, is presented in Fig. S3 in the Supplementary Data.

We firstly focused on the intracellular acetyl-CoA levels of strain

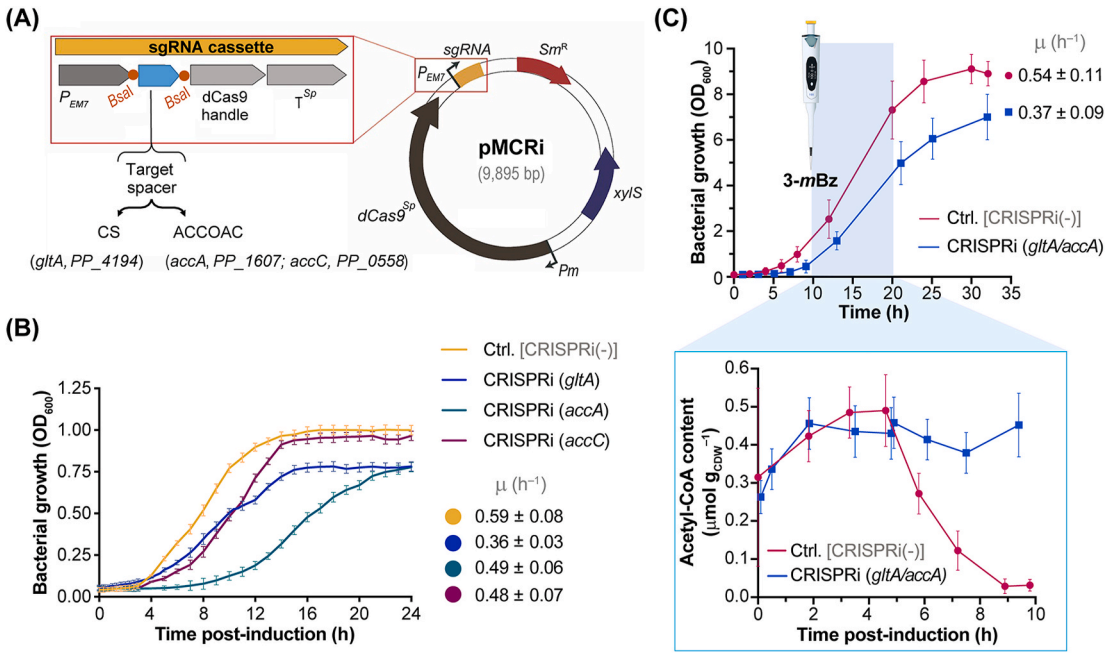

Fig. 2. CRISPRi-mediated gene repression in *P. putida* for boosting acetyl-CoA availability. (A) Schematic representation of vector pMCRi, used for single-guide RNA (sgRNA)-based, 3-methylbenzoate (3-*m*Bz)-inducible CRISPRi. This streptomycin resistant (Sm^R)-vector contains *dCas9*^{Sp} (dead Cas9 gene from *Streptococcus pyogenes*) under control of the XylS/*Pm* expression system and a constitutively-expressed sgRNA cassette. The sgRNA cassette is composed by the synthetic, constitutive P_{EM7} promoter followed by a sgRNA chimera, spanning three domains: a 20-nt region for target-specific binding, a 42-nt hairpin for dCas9 binding (dCas9 handle) and the native 40-nt transcription terminator (T^{Sp}) from *S. pyogenes*. Two *Bsa*I recognition sites have been incorporated between the P_{EM7} promoter and the sgRNA cassette to facilitate cloning of target spacer. **(B)** *P. putida* SEM1.3 was transformed with the empty pMCRi vector [non-target spacer, indicated as CRISPRi(−) and used as a control (Ctrl.)] or with pMCRi plasmids carrying spacers against the *gltA*, *accA* and *accC* sequences (either in single- or multiplex-format, as indicated in the figure). The resulting strains were grown in microtiter plates in 200 μL of de Bont minimal medium supplemented with 0.1% (w/v) glucose, 100 μg mL^{-1} Sm and 1 mM 3-*m*Bz as inducer of the CRISPRi system. Specific growth rates (μ) were calculated during exponential growth based on the optical density at 600 nm (OD_{600}) profiles. **(C)** Growth and acetyl-CoA content in *P. putida* SEM1.3 with dual *accA* and *gltA* repression. Strains SEM 1.3/pMCRi and SEM 1.3/pMCRi_*gltA_accA* were grown in shaken-flask cultures in 50 mL of de Bont minimal medium supplemented with 1% (w/v) glucose, 100 μg mL^{-1} Sm with 1 mM 3-*m*Bz added to the cultures at 10 h to induce CRISPRi-mediated transcriptional repression of *gltA* and *accA*. The acetyl-CoA content, normalized to the biomass (CDW, cell dry weight), was assessed by LC-MS/MS after rapid quenching of cells sampled from these cultures over 10 h after activation of the CRISPRi system. Data points represent the mean value of the corresponding parameter (cell growth or acetyl-CoA content) ± standard deviations of triplicate measurements from at least two independent experiments.

P. putida SEM1.3/pMCRi_*gltA_accA*, with dual CRISPRi knock-down of the two metabolic targets that had the most significant effects on cell physiology (Fig. 2C). The growth profile of both the rewired strain and *P. putida* SEM1.3 transformed with the control vector mirrored the behavior observed in microtiter plate cultures. The control strain grew with $\mu = 0.54 \pm 0.11\ h^{-1}$, whereas the dually *gltA*- and *accA*-repressed strain had a $\mu = 0.37 \pm 0.09\ h^{-1}$, which was further accompanied with a reduction of ca. 25% in the final cell density. The acetyl-CoA levels in both strains followed a similar trend within the first 5 h after addition of 3-*m*Bz to the cultures, reaching ca. 0.5 μmol g_{CDW}^{-1}. After this point, however, the acetyl-CoA content trajectories diverged substantially. While *P. putida* SEM1.3/pMCRi_*gltA_accA* exhibited coenzyme levels virtually constant over the whole time-course experiment (slightly fluctuating around 0.45 μmol g_{CDW}^{-1}, and close to the maximal value indicated above), the acetyl-CoA content in the control strain decreased down to < 0.05 μmol g_{CDW}^{-1} at 10 h post-induction. Thus, the acetyl-CoA content in the rewired strain remained at levels at least 8-fold higher than that in the control strain. This trend was accompanied by a similar behavior in the availability of some metabolites within the TCA cycle (downstream the acetyl-CoA node), especially α-ketoglutarate (Fig. S3 in the Supplementary Data). The isocitrate, malate and succinate content decreased as the cultivation progressed, as observed in rewired *P. putida* strains individually targeting *gltA* or *accA*. Oxaloacetate levels in the rewired strains increased upon activation of the CRISPRi system, as this metabolite is no longer condensed with acetyl-CoA to yield citrate, and then decreased at a latter stage of the cultivation. In the upper metabolism, the 6-phosphogluconate content increased immediately after blocking *accA*; as did the glucose-6-P and fructose-6-P availability upon targeting either *gltA* or *accA*. These manipulations also affected the intracellular pool of some amino acids. CRISPRi-depletion of GltA, for instance, increased the pool of asparagine and (over time) methionine in a similar fashion as observed for oxaloacetate—the metabolite from which these amino acids derive. In addition to this phenomenon, the phenylalanine and tyrosine pools increased significantly (and stably) in rewired strains where *accA* was targeted. These examples show how the network-wide metabolome is fully reshaped upon activation of CRISPRi, providing clues for further manipulations towards bioproduction. Taken together, the quantitative physiology experiments and the metabolomic profiling indicate that the CRISPRi system against *gltA* and *accA* mediates an increase of acetyl-CoA levels in *P. putida* SEM1.3. The next question was whether these manipulations elicited any significant changes in the proteome of the rewired strains.

3.3. Network-wide proteomic analysis reveals a substantial rewiring of central carbon metabolism upon transcriptional repression of gltA and accA

To study the potential changes in metabolism induced by dynamic transcriptional repression in *P. putida*, a comparative proteomic analysis was performed in strains with and without CRISPRi grown in glucose shaken-flask cultures. *P. putida* SEM1.3 carrying the pMCRi vector with a non-target sgRNA was used as a control, whereas strains with plasmids pMCRi_*gltA*, pMCRi_*accA* or pMCRi_*accA_gltA*, mediating the repression

of *gltA* and *accA* either individually or simultaneously, were the test groups. Based on the metabolomic analysis described in the previous section, samples were collected at 10 h after 3-*m*Bz addition (i.e., 20 h after inoculation of the cultures). The protein abundance was compared in the different strains by taking the average values across biological replicates and normalizing the abundances to the control experimental group. Fig. 3 illustrates the normalized protein abundances plotted as heatmaps according to the topology of the biochemical network in Fig. 1A. A principal component analysis of all proteomic data (Fig. S4 in the Supplementary Data) indicated that the individual repression of *gltA* or *accA* resulted in significantly altered levels of 37 and 88 proteins as compared with control experiments, respectively, with a tight false discovery rate <0.01%. Interestingly, dual repression of both *gltA* and *accA* was accompanied by significant changes in the abundance of 332 proteins.

As expected, the proteins directly targeted by the CRISPRi system, GltA (CS) and AccA (carboxyltransferase subunit of the ACCOAC complex), had a lower abundance in *P. putida* SEM1.3/pMCRi_*gltA*, SEM1.3/pMCRi_*accA* and SEM1.3/pMCRi_*gltA*_*accA* as compared to the control experiment (Fig. 3). In the dually-rewired strain, the abundance of both GltA and AccA was <40% of that in the control *P. putida* strain. Other components of the ACCOAC complex, i.e., AccB (biotin-carboxyl carrier unit) and AccC (biotin carboxylase subunit), had a relatively high abundance when the expression of *accA* was targeted by CRISPRi. This effect could be connected to a compensating phenomenon, similarly reported in *E. coli* when genes encoding the individual subunits of the ACCOAC complex are overexpressed (Abdel-Hamid and Cronan, 2007). Interestingly, the highest impact on the abundance of AccA was achieved when *gltA* and *accA* were targeted simultaneously. Such an additive effect was also observed in *P. denitrificans* engineered for 3-hydroxypropionate production (Zhou et al., 2020). In this case, lowering the activities of the TCA cycle *via* cerulenin inhibition increased malonyl-CoA availability by modulating the flux through the ACCOAC complex. Beyond GltA and AccA themselves, we detected a general increase in the abundance of enzymes that could compensate for depletion of the two CRISPRi targets—especially when both of them were knocked-down simultaneously. Such was the case for components of the EDEMP cycle [e.g., the gluconeogenic branch of the Embden-Meyerhof-Parnas (EMP) pathway, including fructose-1,6-P_2 bisphosphatase and glucose-6-P isomerase]. This proteomic pattern fits the observed increase in the steady-state glucose-6-P and fructose-6-P concentrations, and also fructose-1,6-P_2 (Fig. S3 in the Supplementary Data). The peripheral glucose assimilation pathways through oxidation and phosphorylation, i.e., gluconate 2-dehydrogenase, 2-ketogluconate kinase and 2-ketogluconate-6-P reductase, which directly feeds the 6-phosphogluconate node (Volke et al., 2021), were likewise over-represented in rewired strains (which helps explaining the abundance of 6-phosphogluconate detected by metabolomics). The content of enzymes within both the glycolytic branch of the EMP pathway and the Entner-Doudoroff route were also increased (albeit slightly), which probably amplified the conversion of glucose (and their oxidized products) into pyruvate. Substrate availability could, in turn, result in an increase in the PDH complex components (Patel et al., 2014). Interestingly, overexpression of these genes was predicted to increase

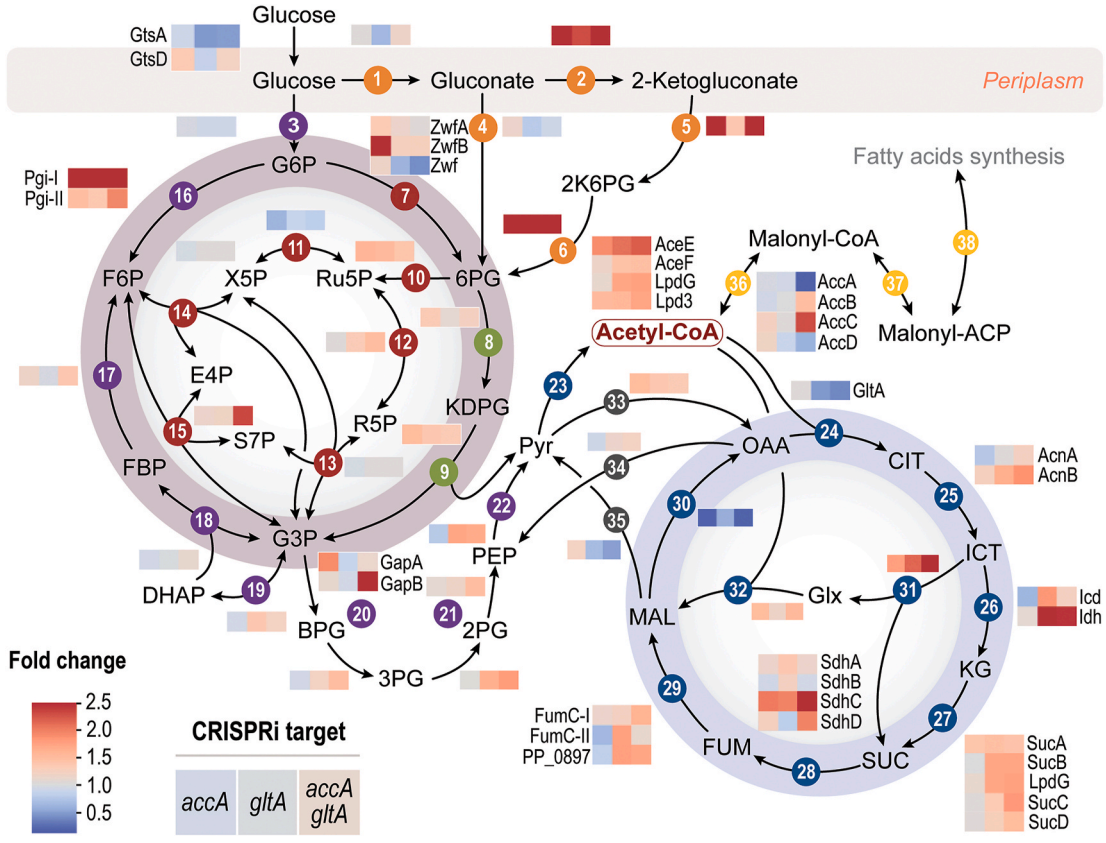

Fig. 3. Comparative network-wide proteomic analysis of CRISPRi-rewired *P. putida* strains. Strain *P. putida* SEM1.3 carrying pMCRi plasmids targeting *accA*, *gltA* or both *accA* and *gltA*, were grown in de Bont minimal medium supplemented with 1% (w/v) glucose, 100 μg mL^{-1} Sm and 1 mM 3-*m*Bz as inducer of the CRISPRi system. *P. putida* SEM1.3 transformed with the empty pMCRi vector (non-target spacer) was used as a control for normalization. The relative protein abundance of enzymes within central carbon metabolism is shown in the plot according to their fold changes during exponential growth. Abundance values were averaged among three biological replicates and normalized to the control strain. When multiple isoforms exist for a given enzyme, they are represented separately, and the individual isozyme names are specified. The heatmap values are shaded to illustrate the effect of transcriptional *gltA* and/or *accA* repression on the respective protein abundance as *grey*, no impact; *red*, positive impact; and blue, negative impact.

acetyl-CoA levels by the kinetic model of *P. putida* (Fig. 1B); hence, depleting GltA and AccA had an indirect effect on the PDH complex that further boosted acetyl-CoA availability in the rewired strains. The compensation effect was also detected in enzymes of the pyruvate shunt in the dually-repressed *P. putida* strain, which connects this metabolite and the TCA cycle in a GltA-independent fashion (Chavarría et al., 2012)—replenishing the lower catabolism to ensure ATP generation. The enzymes of the glyoxylate shunt were significantly affected by these manipulations, probably reflecting a dearth of C2 units that feed the TCA cycle.

Taken together, the results of this network-wide proteomic analysis provide direct evidence of the tuning of protein abundance *via* CRISPRi, which results in diverted carbon fluxes towards enhanced levels of acetyl-CoA—and *P. putida* reacted to this perturbation by adjusting enzyme abundance (and likely, fluxes through them) in central carbon metabolism to counteract the depletion of GltA and AccA. Moreover, gene ontology enrichment analysis in this strain showed increased abundance of proteins in the metabolic routes involved in carbohydrate degradation and acetyl-CoA assimilation, such as purine and amino acid biosynthesis. The detailed gene ontology enrichment analysis is shown in the Supplementary Data (Tables S10–S15 and Figs. S5–S7). As an example, and consistently with previous observations at the level of metabolite profiling (Fig. S3 in the Supplementary Data), enzymes involved in aromatic amino acid biosynthesis had an increased abundance in strains depleted of AccA and GltA, either individually or combined. Enzymes involved in alginate accumulation were likewise over-produced in rewired *P. putida* strains, indicating re-routing of some intermediates (e.g. fructose-6-P, a precursor in the alginate biosynthesis pathway) into the formation of polymeric substances. Other pathway components, in contrast, were significantly downregulated upon interfering with GltA and AccA. A relevant example is the degradation of amino acids that yield acetyl-CoA and components of β-oxidation that would also result in the formation of C2 units for assimilation. In all, this state of affairs opens up the possibility of improving the synthesis of

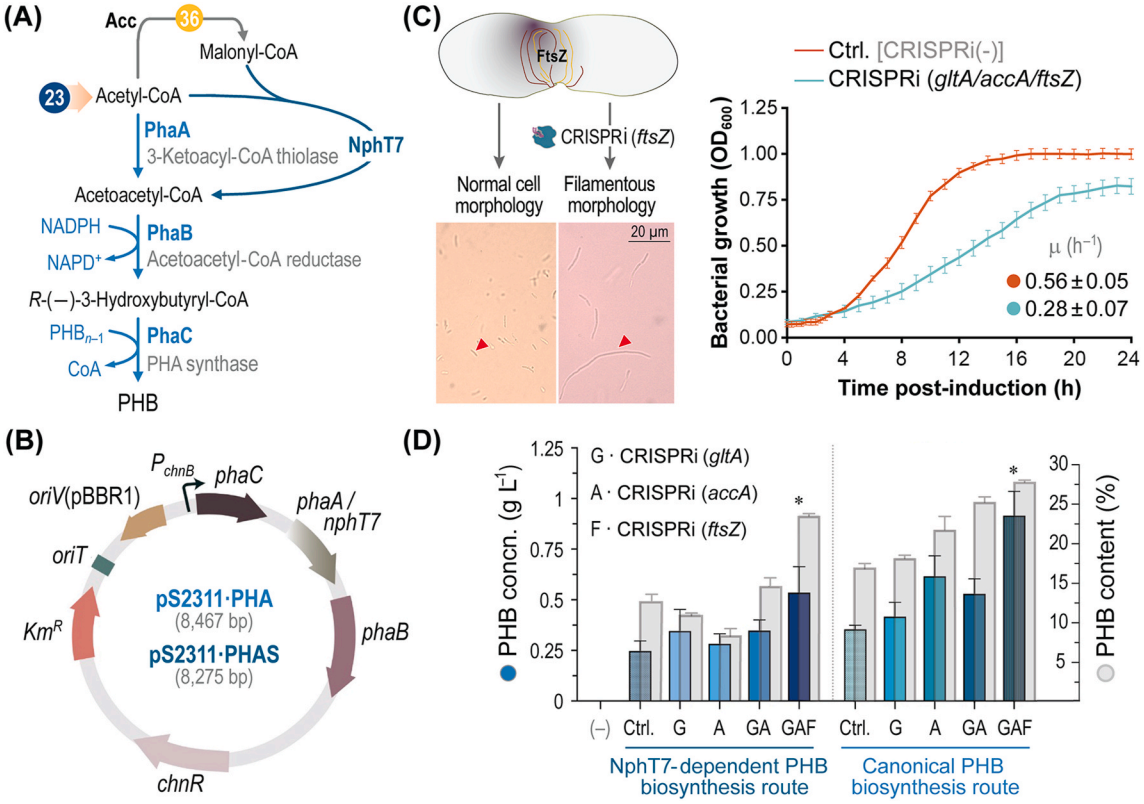

Fig. 4. Engineering synthetic pathways for poly(3-hydroxybutyrate) (PHB) biosynthesis in *P. putida*. **(A)** Canonical and NphT7-dependent PHB biosynthesis routes. In the alternative route, NphT7 mediates the malonyl-CoA–dependent synthesis of acetoacetyl-CoA. The two key reactions producing or consuming acetyl-CoA (citrate synthase, v_{23}, and acetyl-CoA carboxylase, v_{36}, respectively) are identified with their code numbers as in Fig. 1 and were targeted by CRISPRi-mediated knock-down. **(B)** Scheme of plasmids constructed for acetyl-CoA–dependent PHB biosynthesis. The two synthetic pathways differ in the second gene (either *phaA* from *C. necator* in the canonical route or *nphT7* from *Streptomyces* sp. in the alternative route). In either case, the expression of the cognate genes, under control of the ChnR/P_{chnB} system, is triggered by addition of cyclohexanone to the culture medium. Km^R, kanamycin-resistance determinant. **(C)** FtsZ is involved in septum formation during bacterial division and was targeted for manipulating the architecture of PHB-producing *P. putida* cells. *P. putida* SEM1.3 was transformed with the empty pMCRi vector [non-target spacer, indicated as CRISPRi(−) and used as a control (Ctrl.)] or with pMCRi plasmids carrying spacers against the *gltA*, *accA* and *ftsZ* sequences. The resulting strains were grown in de Bont minimal medium supplemented with 1% (w/v) glucose, 100 µg mL^{-1} Sm and 1 mM 3-*m*Bz as inducer of the CRISPRi system. Specific growth rates (µ) were calculated during exponential growth based on the optical density at 600 nm (OD_{600}) profiles. Pictures were taken after 15 h of induction with a Leica 2000 LED microscopy system at 100 × resolution (F1 type immersion oil), and slanted red arrowheads indicate cells displaying a normal morphology or a filamentous phenotype bestowed by transcriptional repression of *ftsZ*. **(D)** PHB production experiments in shaken-flask cultures. *P. putida* SEM1.3 was transformed with a combination of PHB production- and CRISPRi-plasmids as indicated in the figure and grown in de Bont minimal medium supplemented with 1% (w/v) glucose, 50 µg mL^{-1} Km, 100 µg mL^{-1} Sm, 1 mM 3-*m*Bz as inducer of the CRISPRi system and 1 mM cyclohexanone as trigger of PHB accumulation. *P. putida* SEM1.3 transformed with empty vectors (pSEVA2311 and pMCRi) was used as a negative control of accumulation (−), and *P. putida* SEM1.3 transformed with the corresponding PHB production plasmid and the empty pMCRi vector was used as a control of CRISPRi-mediated effects (Ctrl.). The PHB concentration (concn.) was calculated after 24 h of incubation by GC-FID analysis of methanolysed samples. The polymer content, expressed as the % (w/w) of CDW, is represented as grey columns. Bars represent the mean value of the PHB concn. or content ± standard deviations of triplicate measurements from at least three independent experiments, and the asterisk symbol (*) identifies significant differences ($P < 0.01$) between cells carrying the triple-target CRISPRi system and the corresponding Ctrl. experiment.

compounds derived from acetyl-CoA by introducing synthetic pathways that act as a sink for the coenzyme. For the next step of this study, we have chosen PHB accumulation as a model product to explore this hypothesis.

3.4. Design and construction of P. putida strains for PHB accumulation

Considering that PHB biosynthesis starts with acetyl-CoA as the precursor, we adopted this route as a proxy of the effects of rewiring metabolism *via gltA* and *accA* transcriptional repression. To this end, we designed two synthetic routes for PHB biosynthesis, based either on the canonical pathway of *Cupriavidus necator* or on a malonyl-CoA shunt (Fig. 4A). The difference between the two synthetic pathways lies in the first step of the biochemical sequence: in the canonical pathway, two acetyl-CoA molecules are condensed into acetoacetyl-CoA by PhaA, a 3-ketoacyl-CoA thiolase (Anderson and Dawes, 1990). In the alternative route, this biochemical step is replaced by NphT7, an acetoacetyl-CoA synthase from *Streptomyces* sp. that irreversibly condenses acetyl-CoA and malonyl-CoA (Okamura et al., 2010). Hence, this topology enables a further layer of control on precursor availability around the acetyl-CoA and malonyl-CoA metabolic nodes. Using vector pSEVA2311 as the backbone [which bears the tightly-regulated, cyclohexanone-inducible ChnR/P_{chnB} expression system (Benedetti et al., 2016)], two individual plasmids were constructed for PHB synthesis (Fig. 4B). Plasmid pS2311·PHA contains the genes encoding the enzymes of the canonical PHB synthesis route (i.e., PhaC, PhaA and PhaB from *C. necator*), whereas the NphT7-dependent route is borne by plasmid pS2311·PHA, with *nphT7* replacing *phaA*. These plasmids confer PHB biosynthesis upon expression of the cognate genes in glucose cultures of both *E. coli* (data not shown) and *P. putida*, as discussed below.

Building on the use of CRISPRi as an approach to increase acetyl-CoA availability in rewired *P. putida* strains, we added an additional target to boost PHB accumulation. In this case, the knock-down strategy was directed towards cell shape, rather than metabolic targets, in order to tune synthetic morphologies of engineered bacteria (Volke and Nikel, 2018). The bacterial fission ring protein FtsZ is a key player in the formation of the cell septum during the bacterial division process. Down-regulation of *ftsZ* results in the emergence of filamentous cells, which can be beneficial for compounds accumulating inside the cell, e.g., PHB and other polymers (Tao et al., 2017; Zhang et al., 2020). Plasmid pMCRi*_ftsZ* was constructed to target this gene (Table 1) and *P. putida* SEM1.3/pMCRi*_ftsZ* cells acquired a long shape (up to 10-fold longer than normally shaped bacteria), filamentous phenotype upon induction of the CRISPRi with 3-*m*Bz (Fig. 4C). The *ftsZ*-specific spacer was further introduced in plasmid pMCRi*_gltA_accA_ftsZ*, which can be used to repress all three targets simultaneously. Following the trend observed for single- and dually-repressed genes, *P. putida* SEM1.3/pMCRi*_gltA_accA_ftsZ* had a reduction in μ of 50% as compared to the control strain in glucose cultures added with 3-*m*Bz, with final OD_{600} values ranging around 70–80% of those for the control cultures (Fig. 4C). Cells sampled from these experiments showed an altered morphology, where most bacteria had a filamentous morphology (data not shown).

With these metabolic- and morphology engineering CRISPRi system at hand, the next objective was to validate their use for enhanced PHB biosynthesis in rewired *P. putida*. To this end, *P. putida* SEM1.3 was transformed with different combinations of plasmids conferring PHB biosynthesis and mediating CRISPRi of *gltA*, *accA* and *ftsZ* as indicated in Fig. 4D. Shaken-flask cultures of these rewired strains were run in de Bont minimal medium containing glucose as the only carbon source, and biomass and PHB production were measured after 24 h. No PHB accumulation could be detected in strain SEM1.3 carrying the empty pSEVA2311 and pMCRi vectors, used as a negative control here. In contrast, both the NphT7-dependent and the canonical pathways for PHB biosynthesis were effective for polymer accumulation in *P. putida* SEM1.3, with final PHB titers of 0.25 and 0.36 g L^{-1}, respectively. These figures correspond to a PHB content on biomass (on a CDW basis) of 13 and 18%, respectively. Repressing single metabolic targets in *P. putida* SEM1.3 expressing the canonical pathway boosted PHB accumulation by ca. 1.3-fold (in the case of *accA* repression), and a combination of the two (i.e., *P. putida* SEM1.3/pS2311·PHA + pMCRi*_gltA_accA_ftsZ*) further increased the polymer titers by 1.4-fold as compared to those in the control experiment. Addition of the third spacer to the pMCRi plasmids (i.e., repressing *gltA*, *accA* and *ftsZ* simultaneously) further boosted PHB titers by 2.6-fold (reaching a final concentration of ca. 1 g L^{-1}) when compared with the strain without any CRISPRi intervention. A similar qualitative trend was observed in strains carrying the NphT7-dependent route (i.e., *P. putida* SEM1.3/pS2311·PHAS). In this case, the largest impact on PHB titers was brought about by repressing *gltA* that, together with the negligible effect of targeting *accA* on bioproduction, highlights the dual dependence of the NphT7 pathway on acetyl-CoA and malonyl-CoA. Furthermore, *P. putida* SEM1.3/pS2311·PHAS + pMCRi*_gltA_accA_ftsZ* had a 2.2-fold increase in the final PHB titer as compared to its control strain. These results underscore the positive impact of combining metabolic and morphology determinants as targets for CRISPRi—and they show that PHB accumulation can be adopted as a sensitive indicator of acetyl-CoA availability in *P. putida*. On this background, our next task was to study if the rewired strains can be used for acetyl-CoA–dependent biosynthesis in an industrially-relevant cultivation setup.

3.5. CRISPRi-assisted PHB production by rewired P. putida strains in an automated fermentation platform

Considering that few studies have demonstrated the use of CRISPRi as a strategy for increasing product titers and yields in bioreactor cultures, we tested the behavior of the rewired *P. putida* strains in a fully automated, multiplex bioreactor platform. The motivation was assessing if these strains can support consistent PHB biosynthesis during process upscaling while omitting irregularities caused by standard laboratory cultivation formats—where poorly controlled environmental conditions, e.g., pH, temperature drops and aeration, can contribute to significant variations in strain performance (Hecht et al., 2018). To this end, we used the commercial Ambr™ 250 system for process development as a high-throughput, automated bioreactor platform with 12 single-use, 250-mL mini-bioreactors (Fig. 5A)—maintaining the dissolved O_2 tension (dO_2) >40% and controlling the pH at 7 by automatic base addition. Five *P. putida* strains, derived from SEM1.3 and equipped with different plasmid combinations (i.e., pS2311·PHA and CRISPRi plasmids, Fig. 5A), were cultivated in batch-mode in de Bont minimal medium containing 1% (w/v) glucose as the sole carbon source. In these bioreactor experiments, all PHB-producing *P. putida* strains harbored the canonical biosynthesis pathway, selected according to the higher polymer titers it mediated in shaken-flask cultures (Fig. 4D). The dO_2 and carbon evolution rates (CER) trajectories were followed online during the entire cultivation period, and the resulting cultures were harvested after 24–48 h of fermentation for CDW and PHB analysis.

All strains followed a similar qualitative trend in terms of dO_2 and CER curves, indicative of bacterial growth and substrate consumption. The trajectories of *P. putida* SEM1.3 transformed with the empty vectors and the fully rewired strain (SEM1.3/pS2311·PHA + pMCRi*_gltA_accA_ftsZ*) illustrate this behavior (Fig. 5B). Cells started to grow exponentially upon inoculation, marked by a sharp drop in dO_2 accompanied by an increase in CER. Carbon exhaustion at ca. 12 h was signaled by the opposite trend—dO_2 spiked rapidly afterwards, and CO_2 was produced at very low CERs. Biomass and PHB were likewise determined in samples of these cultures (Fig. 5C). On one hand, *P. putida* SEM1.3/pS2311·PHA + empty pMCRi vector, the control strain, produced 0.27 g L^{-1} of PHB, which corresponds to a biopolymer accumulation of 17% (w/w) on a CDW basis—similarly to the results obtained in shaken-flask cultures (Fig. 4D). The rewired *P. putida* strains, on the other hand, featured increased PHB titers and polymer accumulation profiles. *P. putida*

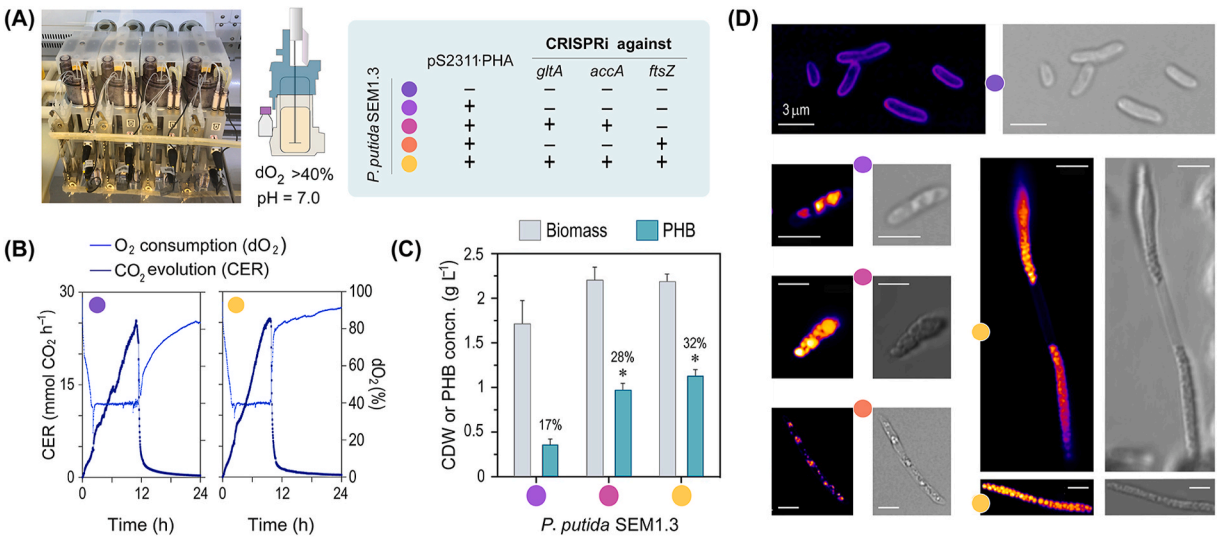

Fig. 5. Poly(3-hydroxybutyrate) (PHB) biosynthesis in rewired *P. putida* strains in automated bioreactor cultures. (A) The Ambr™ 250 bioreactor system was used for controlled cultivation of the *P. putida* strains (derived from *P. putida* SEM1.3) indicated in the table. The same color code identifies the different strains in all panels of this figure. Batch-mode fermentations were carried out in de Bont minimal medium with 1% (w/v) glucose as the carbon source, 1 mM 3-*m*Bz for induction of the CRISPRi system, 1 mM cyclohexanone as a trigger of PHB biosynthesis, 100 µg mL^{-1} streptomycin and 50 µg mL^{-1} kanamycin. All fermentations were performed in independent biological triplicates, and the dissolved O_2 tension (dO_2) and pH were automatically controlled during the runs as indicated. **(B)** Representative fermentation profiles for two of the *P. putida* strains analyzed (control strain, and fully rewired *P. putida* SEM1.3). O_2 consumption (represented as the dO_2) and CO_2 evolution rates (CER) were recorded online with the built-in Ambr™ 250 bioreactor system software. **(C)** Biomass (cell dry weight, CDW) and PHB concentration (concn.) in cultures of rewired *P. putida* SEM1.3 at 24 h. Polymer accumulation is also shown as the PHB content in % (w/w) of the cell dry weight. Bars represent the mean value of either the CDW or PHB concns. ± standard deviations of triplicate measurements from at least three independent bioreactor experiments, the asterisk symbol (*) identifies significant differences ($P < 0.01$) with respect to *P. putida* SEM1.3/pS2311·PHA + empty pMCRi vector. **(D)** Morphology phenotypes of rewired *P. putida* SEM1.3 cells sampled from bioreactor cultures after 24 h. Representative pictures were taken in a high-resolution laser scanning confocal microscopy system after staining the cells with a 0.5 µg mL^{-1} Nile Red solution to detect intracellular PHB granules (Spiekermann et al., 1999). The scale of the microscopy pictures is shown with a white line and represents 3 µm in all cases.

SEM1.3/pS2311·PHA + pMCRi_*gltA_accA* reached a PHB concentration of 0.94 g L^{-1}, with a polymer accumulation of 28% (w/w). When synthetic morphology was also targeted by CRISPRi (i.e., cells carrying plasmid pMCRi_*gltA_accA_ftsZ*), the rewired strain *P. putida* produced 1.12 g L^{-1} of PHB—reaching the highest polymer accumulation of 32% (w/w), which corresponds to a 5-fold increase with respect to the control, non-CRISPRi strain.

High-resolution laser scanning confocal microscopy of *P. putida* cells harvested from these bioreactor cultures exposed bacterial phenotypes upon PHB accumulation (Fig. 5D). Intracellular PHB granules were dyed *in vivo* by using a viable-staining procedure. Expectedly, no PHB accumulation was observed in strain SEM1.3 carrying the empty pSEVA2311 and pMCRi vectors, used here as a negative control. Cells carrying plasmid pS2311·PHA, in contrast, accumulated amorphous PHB inclusions (easily discernible as bright orange spots in the cytoplasm). The effect of targeting the two metabolic enzymes (i.e., CS and ACCOAC) was clearly discernible in *P. putida* SEM1.3/pS2311·PHA + pMCRi_*gltA_accA* cells, as the number and size of intracellular PHB inclusions was significantly increased when compared to the non-CRISPRi strain. Suppressing *ftsZ* expression had a strong impact on bacterial shape—as we could observe the elongated, filamentous cell phenotype previously detected by simpler, contrast-phase microscopy observation (Fig. 4C). Finally, fully rewired *P. putida* cells exhibited an altered morphology and were essentially filled with PHB inclusions—in agreement with the direct determination of PHB accumulation in samples from these cultures (Fig. 5C).

4. Conclusion

The unavoidable competition between biomass accumulation and production of target compounds is a well-recognized challenge in biomanufacturing—and such trade-off impacts (often, limiting) both product titers and bioprocess scalability (Fernández-Cabezón et al., 2019). Such problem becomes particularly relevant for products derived from central metabolites, which could be either converted to biomass components or the compound(s) of interest. Thus, manipulating metabolic nodes to redirect fluxes from these central precursor metabolites towards bioproduction is key towards establishing robust cell factories (Nielsen and Keasling, 2016). Canonical approaches for prediction of targets for manipulation include flux balance analysis-guided methods based on genome-scale or kinetic models and metabolic control analysis based on kinetic models (Banerjee et al., 2020; Gopalakrishnan et al., 2020; Lloyd et al., 2018; Maia et al., 2016). Kinetic ensemble modelling has been recently shown to be very useful in predicting the impact of metabolic perturbations in *P. putida* KT2440 (Tokic et al., 2020). In their contribution, the authors created a near-genome scale kinetic model capable of capturing complex phenotypes (e.g., ATP demand and redox homeostasis) under different growth conditions and *via* the *in silico* implementation of key knock-outs. In this work, we focused on developing a kinetic model rooted on central carbon metabolism and containing a detailed description of reaction kinetics. Our core kinetic model of central carbon metabolism in *P. putida* was developed by rationally integrating fluxomics, thermodynamics and metabolomics datasets—in addition to manually-curated information of enzyme mechanisms, number of composing subunits and allosteric inhibitors and activators. The modelling strategy adopted herein highlighted the (surprisingly few) crucial reactions of central carbon metabolism that should be targeted to improve acetyl-CoA availability in *P. putida*. Knock-down of essential genes—e.g., *accA*, as suggested by the model—can only be performed by dynamic regulation of gene transcription (Brockman and Prather, 2015). In this sense, CRISPRi emerged as a powerful technique to establish balanced metabolic networks with rerouted fluxes towards desired products, especially when genome-wide transcriptional regulation is required (Larson et al., 2013). In recent years, a variety of metabolic engineering applications leveraged CRISPRi to increase the titer and productivity of several primary and

secondary bioproducts, e.g. terpenes (Tao et al., 2018), organic acids (Woolston et al., 2018) and amino acids (Cleto et al., 2016). We followed a similar approach by rewiring the acetyl-CoA node *via* CRISPRi—not only at the level of metabolic enzymes, but also to establish synthetic morphologies that facilitated the accumulation of an intracellular polymer (i.e. PHB, produced *via* two synthetic pathways). Our approach adds to some studies that showed how the manipulation of cell morphologies in engineered *E. coli* and *Halomonas* had a significant and positive effect on PHA accumulation (Jiang and Chen, 2016; Jiang et al., 2015). In these examples, CRISPRi was adopted to tamper with cell wall synthesis- or cell shape-determining proteins, as loosening the cells rigidity improved PHB accumulation (Chen and Jiang, 2017; Zhang et al., 2018). From a broader perspective, repressing the transcription of genes that encode key enzymes or structural proteins can be used to assess the interplay between essentiality towards decoupling growth from production of the desired compound(s). Strategies of this sort will also support the development of efficient bioprocesses at scale when using microbial species that are difficult to grow in high-cell-density (e.g., fed-batch) culture setups. Moreover, this type of combined, *in silico*--guided approach will enable access to non-biological, added-value products (Calero et al., 2020; Nieto-Domínguez and Nikel, 2020) as the expanding synthetic biology toolbox facilitates the engineering of non-traditional cell factories towards *neo*-metabolism.

CRediT authorship contribution statement

Ekaterina Kozaeva: Conceptualization, Investigation, Data curation, Methodology, Validation, Visualization, Writing – original draft. **Svetlana Volkova:** Investigation, Data curation, Visualization, Writing – original draft. **Marta R.A. Matos:** Data curation, Methodology, Validation, Writing – original draft. **Mariela P. Mezzina:** Investigation, Data curation, Methodology. **Tune Wulff:** Data curation, Methodology. **Daniel C. Volke:** Data curation, Methodology. **Lars K. Nielsen:** Conceptualization, Supervision, Writing – review & editing. **Pablo I. Nikel:** Conceptualization, Resources, Data curation, Funding acquisition, Supervision, Project administration, Writing – review & editing.

Declaration of competing interest

The authors have no competing interest to declare.

Acknowledgments

We are thankful to Ivan Kulik, Suresh Sudarsan, Christoffer Knudsen and Milica Randelovic for experimental support, fruitful discussions and technical assistance. The financial support from The Novo Nordisk Foundation through grants NNF20CC0035580, *LiFe* (NNF18OC0034818) and *TARGET* (NNF21OC0067996), the Danish Council for Independent Research (*SWEET*, DFF-Research Project 8021-00039B), and the European Union's Horizon 2020 Research and Innovation Programme under grant agreement No. 814418 (*SinFonia*) to P.I. N. is gratefully acknowledged. E.K. and S.V. were supported by the Novo Nordisk Foundation (grant NNF17CC0026768) as part of the Copenhagen Bioscience Ph.D. Programme. M.P.M. acknowledges the support of the Novo Nordisk Foundation through a post-doctoral fellowship (grant NNF18OC0032314).

Appendix A. Supplementary data

Supplementary data to this article can be found online at https://doi.org/10.1016/j.ymben.2021.07.014.

References

Abdel-Hamid, A.M., Cronan, J.E., 2007. Coordinate expression of the acetyl coenzyme A carboxylase genes, *accB* and *accC*, is necessary for normal regulation of biotin synthesis in *Escherichia coli*. J. Bacteriol. 189, 369–376.

Akkaya, Ö., Pérez-Pantoja, D., Calles, B., Nikel, P.I., de Lorenzo, V., 2018. The metabolic redox regime of *Pseudomonas putida* tunes its evolvability toward novel xenobiotic substrates. mBio 9, e01512–18.

Anderson, A.J., Dawes, E.A., 1990. Occurrence, metabolism, metabolic role, and industrial uses of bacterial polyhydroxyalkanoates. Microbiol. Rev. 54, 450–472.

Bagdasarian, M., Lurz, R., Rückert, B., Franklin, F.C.H., Bagdasarian, M.M., Frey, J., Timmis, K.N., 1981. Specific purpose plasmid cloning vectors. II. Broad host range, high copy number, RSF1010-derived vectors, and a host-vector system for gene cloning in *Pseudomonas*. Gene 16, 237–247.

Banerjee, D., Eng, T., Lau, A.K., Sasaki, Y., Wang, B., Chen, Y., Prahl, J.P., Singan, V.R., Herbert, R.A., Liu, Y., Tanjore, D., Petzold, C.J., Keasling, J.D., Mukhopadhyay, A., 2020. Genome-scale metabolic rewiring improves titers rates and yields of the non-native product indigoidine at scale. Nat. Commun. 11, 5385.

Barajas, J.F., Blake-Hedges, J.M., Bailey, C.B., Curran, S., Keasling, J.D., 2017. Engineered polyketides: synergy between protein and host level engineering. Synth. Syst. Biotechnol. 2, 147–166.

Batianis, C., Kozaeva, E., Damalas, S.G., Martín-Pascual, M., Volke, D.C., Nikel, P.I., Martins dos Santos, V.A.P., 2020. An expanded CRISPRi toolbox for tunable control of gene expression in *Pseudomonas putida*. Microb. Biotechnol. 13, 368–385.

Becker, J., Wittmann, C., 2018. From systems biology to metabolically engineered cells–An omics perspective on the development of industrial microbes. Curr. Opin. Microbiol. 45, 180–188.

Beckers, V., Poblete-Castro, I., Tomasch, J., Wittmann, C., 2016. Integrated analysis of gene expression and metabolic fluxes in PHA-producing *Pseudomonas putida* grown on glycerol. Microb. Cell Factories 15, 73.

Belda, E., van Heck, R.G.A., López-Sánchez, M.J., Cruveiller, S., Barbe, V., Fraser, C., Klenk, H.P., Petersen, J., Morgat, A., Nikel, P.I., Vallenet, D., Rouy, Z., Sekowska, A., Martins dos Santos, V.A.P., de Lorenzo, V., Danchin, A., Médigue, C., 2016. The revisited genome of *Pseudomonas putida* KT2440 enlightens its value as a robust metabolic *chassis*. Environ. Microbiol. 18, 3403–3424.

Benedetti, I., de Lorenzo, V., Nikel, P.I., 2016. Genetic programming of catalytic *Pseudomonas putida* biofilms for boosting biodegradation of haloalkanes. Metab. Eng. 33, 109–118.

Bentley, G.J., Narayanan, N., Jha, R.K., Salvachúa, D., Elmore, J.R., Peabody, G.L., Black, B.A., Ramírez, K., de Capite, A., Michener, W.E., Werner, A.Z., Klingeman, D. M., Schindel, H.S., Nelson, R., Foust, L., Guss, A.M., Dale, T., Johnson, C.W., Beckham, G.T., 2020. Engineering glucose metabolism for enhanced muconic acid production in *Pseudomonas putida* KT2440. Metab. Eng. 59, 64–75.

Bitzenhofer, N.L., Kruse, L., Thies, S., Wynands, B., Lechtenberg, T., Rönitz, J., Kozaeva, E., Wirth, N.T., Eberlein, C., Jaeger, K.E., Nikel, P.I., Heipieper, H.J., Wierckx, N., Loeschcke, A., 2021. Towards robust *Pseudomonas* cell factories to harbour novel biosynthetic pathways. Essays Biochem. 65, 319–336.

Bongers, M., Pérez-Gil, J., Hodson, M.P., Schrübbers, L., Wulff, T., Sommer, M.O.A., Nielsen, L.K., Vickers, C.E., 2020. Adaptation of hydroxymethylbutenyl diphosphate reductase enables volatile isoprenoid production. eLife 9, e48685.

Braunegg, G., Sonnleitner, B., Lafferty, R.M., 1978. A rapid gas chromatographic method for the determination of poly-β-hydroxybutyric acid in microbial biomass. Eur. J. Appl. Microbiol. Biotechnol. 6, 29–37.

Brockman, I.M., Prather, K.L.J., 2015. Dynamic knockdown of *E. coli* central metabolism for redirecting fluxes of primary metabolites. Metab. Eng. 28, 104–113.

Calero, P., Nikel, P.I., 2019. Chasing bacterial *chassis* for metabolic engineering: a perspective review from classical to non-traditional microorganisms. Microb. Biotechnol. 12, 98–124.

Calero, P., Volke, D.C., Lowe, P.T., Gotfredsen, C.H., O'Hagan, D., Nikel, P.I., 2020. A fluoride-responsive genetic circuit enables *in vivo* biofluorination in engineered *Pseudomonas putida*. Nat. Commun. 11, 5045.

Cavaleiro, A.M., Kim, S.H., Seppälä, S., Nielsen, M.T., Nørholm, M.H., 2015. Accurate DNA assembly and genome engineering with optimized uracil excision cloning. ACS Synth. Biol. 4, 1042–1046.

Chavarría, M., Kleijn, R.J., Sauer, U., Pflüger-Grau, K., de Lorenzo, V., 2012. Regulatory tasks of the phosphoenolpyruvate-phosphotransferase system of *Pseudomonas putida* in central carbon metabolism. mBio 3, e00028–12.

Chavarría, M., Nikel, P.I., Pérez-Pantoja, D., de Lorenzo, V., 2013. The Entner-Doudoroff pathway empowers *Pseudomonas putida* KT2440 with a high tolerance to oxidative stress. Environ. Microbiol. 15, 1772–1785.

Chen, G.Q., Jiang, X.R., 2017. Engineering microorganisms for improving polyhydroxyalkanoate biosynthesis. Curr. Opin. Biotechnol. 53, 20–25.

Chen, Y., Banerjee, D., Mukhopadhyay, A., Petzold, C.J., 2020. Systems and synthetic biology tools for advanced bioproduction hosts. Curr. Opin. Biotechnol. 64, 101–109.

Chohnan, S., Furukawa, H., Fujio, T., Nishihara, H., Takamura, Y., 1997. Changes in the size and composition of intracellular pools of nonesterified coenzyme A and coenzyme A thioesters in aerobic and facultatively anaerobic bacteria. Appl. Environ. Microbiol. 63, 553–560.

Choi, K.R., Jang, W.D., Yang, D., Cho, J.S., Park, D., Lee, S.Y., 2019. Systems metabolic engineering strategies: integrating systems and synthetic biology with metabolic engineering. Trends Biotechnol. 37, 817–837.

Choi, S.Y., Rhie, M.N., Kim, H.T., Joo, J.C., Cho, I.J., Son, J., Jo, S.Y., Sohn, Y.J., Baritugo, K.A., Pyo, J., Lee, Y., Lee, S.Y., Park, S.J., 2020. Metabolic engineering for the synthesis of polyesters: a 100-year journey from polyhydroxyalkanoates to non-natural microbial polyesters. Metab. Eng. 58, 47–81.

Choi, Y.J., Morel, L., Bourque, D., Mullick, A., Massie, B., Míguez, C.B., 2006. Bestowing inducibility on the cloned methanol dehydrogenase promoter (P_{mxaF}) of *Methylobacterium extorquens* by applying regulatory elements of *Pseudomonas putida* F1. Appl. Environ. Microbiol. 72, 7723–7729.
Cleland, W.W., 1963. The kinetics of enzyme-catalyzed reactions with two or more substrates or products. III. Prediction of initial velocity and inhibition patterns by inspection. Biochim. Biophys. Acta 67, 188–196.
Cleto, S., Jensen, J.V., Wendisch, V.F., Lu, T.K., 2016. *Corynebacterium glutamicum* metabolic engineering with CRISPR interference (CRISPRi). ACS Synth. Biol. 5, 375–385.
Domínguez, A.A., Lim, W.A., Qi, L.S., 2016. Beyond editing: repurposing CRISPR-Cas9 for precision genome regulation and interrogation. Nat. Rev. Mol. Cell Biol. 17, 5–15.
Eng, T., Banerjee, D., Lau, A.K., Bowden, E., Herbert, R.A., Trinh, J., Prahl, J.P., Deutschbauer, A., Tanjore, D., Mukhopadhyay, A., 2021. Engineering *Pseudomonas putida* for efficient aromatic conversion to bioproduct using high throughput screening in a bioreactor. Metab. Eng. 66, 229–238.
Fang, X., Lloyd, C.J., Palsson, B.Ø., 2020. Reconstructing organisms *in silico*: genome-scale models and their emerging applications. Nat. Rev. Microbiol. 18, 731–743.
Feist, C.F., Hegeman, G.D., 1969. Phenol and benzoate metabolism by *Pseudomonas putida*: regulation of tangential pathways. J. Bacteriol. 100, 869–877.
Fernández-Cabezón, L., Cros, A., Nikel, P.I., 2019. Evolutionary approaches for engineering industrially-relevant phenotypes in bacterial cell factories. Biotechnol. J. 14, 1800439.
Ferreira, J.A., 2007. The Benjamini-Hochberg method in the case of discrete test statistics. Int. J. Biostat. 3, 11.
Flamholz, A., Noor, E., Bar-Even, A., Milo, R., 2012. *e*Quilibrator—the biochemical thermodynamics calculator. Nucleic Acids Res. 40, D770–D775.
Gauttam, R., Mukhopadhyay, A., Simmons, B.A., Singer, S.W., 2021. Development of dual-inducible duet-expression vectors for tunable gene expression control and CRISPR interference-based gene repression in *Pseudomonas putida* KT2440. Microb. Biotechnol. https://doi.org/10.1111/1751-7915.13832 (in press).
Genee, H.J., Bonde, M.T., Bagger, F.O., Jespersen, J.B., Sommer, M.O.A., Wernersson, R., Olsen, L.R., 2015. Software-supported *USER* cloning strategies for site-directed mutagenesis and DNA assembly. ACS Synth. Biol. 4, 342–349.
Gläser, L., Kuhl, M., Jovanovic, S., Fritz, M., Vögeli, B., Erb, T.J., Becker, J., Wittmann, C., 2020. A common approach for absolute quantification of short chain CoA thioesters in prokaryotic and eukaryotic microbes. Microb. Cell Fact. 19, 160.
Gopalakrishnan, S., Dash, S., Maranas, C., 2020. K-FIT: an accelerated kinetic parameterization algorithm using steady-state fluxomic data. Metab. Eng. 61, 197–205.
Hanahan, D., Meselson, M., 1983. Plasmid screening at high colony density. Methods Enzymol. 100, 333–342.
Hartmans, S., Smits, J.P., van der Werf, M.J., Volkering, F., de Bont, J.A., 1989. Metabolism of styrene oxide and 2-phenylethanol in the styrene-degrading *Xanthobacter* strain 124X. Appl. Environ. Microbiol. 55, 2850–2855.
Hecht, A., Filliben, J., Munro, S.A., Salit, M., 2018. A minimum information standard for reproducing bench-scale bacterial cell growth and productivity. Commun. Biol. 1, 219.
Hunter, J.D., 2007. Matplotlib: a 2D graphics environment. Comput. Sci. Eng. 9, 90–95.
Jakočiūnas, T., Jensen, M.K., Keasling, J.D., 2017. System-level perturbations of cell metabolism using CRISPR/Cas9. Curr. Opin. Biotechnol. 46, 134–140.
Jiang, X.R., Chen, G.Q., 2016. Morphology engineering of bacteria for bio-production. Biotechnol. Adv. 34, 435–440.
Jiang, X.R., Wang, H., Shen, R., Chen, G.Q., 2015. Engineering the bacterial shapes for enhanced inclusion bodies accumulation. Metab. Eng. 29, 227–237.
Jiménez, J.I., Miñambres, B., García, J.L., Díaz, E., 2002. Genomic analysis of the aromatic catabolic pathways from *Pseudomonas putida* KT2440. Environ. Microbiol. 4, 824–841.
Jiménez, J.I., Pérez-Pantoja, D., Chavarría, M., Díaz, E., de Lorenzo, V., 2014. A second chromosomal copy of the *catA* gene endows *Pseudomonas putida* mt-2 with an enzymatic safety valve for excess of catechol. Environ. Microbiol. 16, 1767–1778.
Karp, P.D., Billington, R., Holland, T.A., Kothari, A., Krummenacker, M., Weaver, D., Latendresse, M., Paley, S., 2015. Computational metabolomics operations at BioCyc.org. Metabolites 5, 291–310.
Kiefer, D., Merkel, M., Lilge, L., Henkel, M., Hausmann, R., 2021. From acetate to bio-based products: underexploited potential for industrial biotechnology. Trends Biotechnol. 39, 397–411.
Kim, S.K., Yoon, P.K., Kim, S.J., Woo, S.G., Rha, E., Lee, H., Yeom, S.J., Kim, H., Lee, D. H., Lee, S.G., 2020. CRISPR interference-mediated gene regulation in *Pseudomonas putida* KT2440. Microb. Biotechnol. 13, 210–221.
Ko, Y.S., Kim, J.W., Lee, J.A., Han, T., Kim, G.B., Park, J.E., Lee, S.Y., 2020. Tools and strategies of systems metabolic engineering for the development of microbial cell factories for chemical production. Chem. Soc. Rev. 49, 4615–4636.
Ku, J.T., Chen, A.Y., Lan, E.I., 2020. Metabolic engineering design strategies for increasing acetyl-CoA flux. Metabolites 10, 166.
Lammens, E.M., Nikel, P.I., Lavigne, R., 2020. Exploring the synthetic biology potential of bacteriophages for engineering non-model bacteria. Nat. Commun. 11, 5294.
Larson, M.H., Gilbert, L.A., Wang, X., Lim, W.A., Weissman, J.S., Qi, L.S., 2013. CRISPR interference (CRISPRi) for sequence-specific control of gene expression. Nat. Protoc. 8, 2180–2196.
Lewis, N.E., Hixson, K.K., Conrad, T.M., Lerman, J.A., Charusanti, P., Polpitiya, A.D., Adkins, J.N., Schramm, G., Purvine, S.O., López-Ferrer, D., Weitz, K.K., Eils, R., König, R., Smith, R.D., Palsson, B.Ø., 2010. Omic data from evolved *E. coli* are consistent with computed optimal growth from genome-scale models. Mol. Syst. Biol. 6, 390.
Lloyd, C.J., Ebrahim, A., Yang, L., King, Z.A., Catoiu, E., O'Brien, E.J., Liu, J.K., Palsson, B.Ø., 2018. *COBRAme*: a computational framework for genome-scale models of metabolism and gene expression. PLoS Comput. Biol. 14, e1006302.
Loeschcke, A., Thies, S., 2015. *Pseudomonas putida*–A versatile host for the production of natural products. Appl. Microbiol. Biotechnol. 99, 6197–6214.
Maia, P., Rocha, M., Rocha, I., 2016. *In silico* constraint-based strain optimization methods: the quest for optimal cell factories. Microbiol. Mol. Biol. Rev. 80, 45–67.
Martínez-García, E., Aparicio, T., de Lorenzo, V., Nikel, P.I., 2014a. New transposon tools tailored for metabolic engineering of Gram-negative microbial cell factories. Front. Bioeng. Biotechnol. 2, 46.
Martínez-García, E., Nikel, P.I., Aparicio, T., de Lorenzo, V., 2014b. *Pseudomonas* 2.0: genetic upgrading of *P. putida* KT2440 as an enhanced host for heterologous gene expression. Microb. Cell Factories 13, 159.
McCloskey, D., Young, J.D., Xu, S., Palsson, B.Ø., Feist, A.M., 2016. MID Max: LC–MS/MS method for measuring the precursor and product mass isotopomer distributions of metabolic intermediates and cofactors for metabolic flux analysis applications. Anal. Chem. 88, 1362–1370.
Mezzina, M.P., Manoli, M.T., Prieto, M.A., Nikel, P.I., 2021. Engineering native and synthetic pathways in *Pseudomonas putida* for the production of tailored polyhydroxyalkanoates. Biotechnol. J. 16, 2000165.
Moreno-Sánchez, R., Saavedra, E., Rodríguez-Enríquez, S., Olín-Sandoval, V., 2008. Metabolic control analysis: a tool for designing strategies to manipulate metabolic pathways. J. Biomed. Biotechnol. 2008, 597913.
Nielsen, J., Keasling, J.D., 2016. Engineering cellular metabolism. Cell 164, 1185–1197.
Nieto-Domínguez, M., Nikel, P.I., 2020. Intersecting xenobiology and *neo*-metabolism to bring novel chemistries to life. Chembiochem 21, 2551–2571.
Nikel, P.I., Pettinari, M.J., Galvagno, M.A., Méndez, B.S., 2006. Poly(3-hydroxybutyrate) synthesis by recombinant *Escherichia coli arcA* mutants in microaerobiosis. Appl. Environ. Microbiol. 72, 2614–2620.
Nikel, P.I., Chavarría, M., Fuhrer, T., Sauer, U., de Lorenzo, V., 2015. *Pseudomonas putida* KT2440 strain metabolizes glucose through a cycle formed by enzymes of the Entner-Doudoroff, Embden-Meyerhof-Parnas, and pentose phosphate pathways. J. Biol. Chem. 290, 25920–25932.
Nikel, P.I., Fuhrer, T., Chavarría, M., Sánchez-Pascuala, A., Sauer, U., de Lorenzo, V., 2021. Reconfiguration of metabolic fluxes in *Pseudomonas putida* as a response to sub-lethal oxidative stress. ISME J. 15, 1751–1766.
Nikel, P.I., de Lorenzo, V., 2018. *Pseudomonas putida* as a functional *chassis* for industrial biocatalysis: from native biochemistry to *trans*-metabolism. Metab. Eng. 50, 142–155.
Nishida, K., Kondo, A., 2020. CRISPR-derived genome editing technologies for metabolic engineering. Metab. Eng. 63, 141–147.
Nogales, J., Mueller, J., Gudmundsson, S., Canalejo, F.J., Duque, E., Monk, J., Feist, A. M., Ramos, J.L., Niu, W., Palsson, B.Ø., 2020. High-quality genome-scale metabolic modelling of *Pseudomonas putida* highlights its broad metabolic capabilities. Environ. Microbiol. 22, 255–269.
Okamura, E., Tomita, T., Sawa, R., Nishiyama, M., Kuzuyama, T., 2010. Unprecedented acetoacetyl-coenzyme A synthesizing enzyme of the thiolase superfamily involved in the mevalonate pathway. Proc. Natl. Acad. Sci. U.S.A. 107, 11265–11270.
Patel, M.S., Nemeria, N.S., Furey, W., Jordan, F., 2014. The pyruvate dehydrogenase complexes: structure-based function and regulation. J. Biol. Chem. 289, 16615–16623.
Poblete-Castro, I., Wittmann, C., Nikel, P.I., 2020. Biochemistry, genetics, and biotechnology of glycerol utilization in *Pseudomonas* species. Microb. Biotechnol. 13, 32–53.
Polyak, S.W., Abell, A.D., Wilce, M.C.J., Zhang, L., Booker, G.W., 2012. Structure, function and selective inhibition of bacterial acetyl-CoA carboxylase. Appl. Microbiol. Biotechnol. 93, 983–992.
Prieto, M.A., Escapa, I.F., Martínez, V., Dinjaski, N., Herencias, C., de la Peña, F., Tarazona, N., Revelles, O., 2016. A holistic view of polyhydroxyalkanoate metabolism in *Pseudomonas putida*. Environ. Microbiol. 18, 341–357.
Rabinowitz, J.D., Kimball, E., 2007. Acidic acetonitrile for cellular metabolome extraction from *Escherichia coli*. Anal. Chem. 79, 6167–6173.
Ruiz, J.A., Fernández, R.O., Nikel, P.I., Méndez, B.S., Pettinari, M.J., 2006. *dye* (*arc*) Mutants: insights into an unexplained phenotype and its suppression by the synthesis of poly(3-hydroxybutyrate) in *Escherichia coli* recombinants. FEMS Microbiol. Lett. 258, 55–60.
Saa, P., Nielsen, L.K., 2015. A general framework for thermodynamically consistent parameterization and efficient sampling of enzymatic reactions. PLoS Comput. Biol. 11, e1004195.
Salvachúa, D., Rydzak, T., Auwae, R., De Capite, A., Black, B.A., Bouvier, J.T., Cleveland, N.S., Elmore, J.R., Huenemann, J.D., Katahira, R., Michener, W.E., Peterson, D.J., Rohrer, H., Vardon, D.R., Beckham, G.T., Guss, A.M., 2020. Metabolic engineering of *Pseudomonas putida* for increased polyhydroxyalkanoate production from lignin. Microb. Biotechnol. 13, 290–298.
Sánchez-Pascuala, A., Fernández-Cabezón, L., de Lorenzo, V., Nikel, P.I., 2019. Functional implementation of a linear glycolysis for sugar catabolism in *Pseudomonas putida*. Metab. Eng. 54, 200–211.
Schultenkämper, K., Brito, L.F., Wendisch, V.F., 2020. Impact of CRISPR interference on strain development in biotechnology. Biotechnol. Appl. Biochem. 67, 7–21.
Shen, X., Wang, J., Li, C., Yuan, Q., Yan, Y., 2019. Dynamic gene expression engineering as a tool in pathway engineering. Curr. Opin. Biotechnol. 59, 122–129.
Silva-Rocha, R., Martínez-García, E., Calles, B., Chavarría, M., Arce-Rodríguez, A., de las Heras, A., Páez-Espino, A.D., Durante-Rodríguez, G., Kim, J., Nikel, P.I., Platero, R., de Lorenzo, V., 2013. The Standard European Vector Architecture (SEVA): a coherent platform for the analysis and deployment of complex prokaryotic phenotypes. Nucleic Acids Res. 41, D666–D675.

Smanski, M.J., Zhou, H., Claesen, J., Shen, B., Fischbach, M.A., Voigt, C.A., 2016. Synthetic biology to access and expand nature's chemical diversity. Nat. Rev. Microbiol. 14, 135–149.
Smith, A.C., Cronan, J.E., 2012. Dimerization of the bacterial biotin carboxylase subunit is required for acetyl coenzyme A carboxylase activity *in vivo*. J. Bacteriol. 194, 72–78.
Spiekermann, P., Rehm, B.H., Kalscheuer, R., Baumeister, D., Steinbüchel, A., 1999. A sensitive, viable-colony staining method using Nile red for direct screening of bacteria that accumulate polyhydroxyalkanoic acids and other lipid storage compounds. Arch. Microbiol. 171, 73–80.
Sudarsan, S., Dethlefsen, S., Blank, L.M., Siemann-Herzberg, M., Schmid, A., 2014. The functional structure of central carbon metabolism in *Pseudomonas putida* KT2440. Appl. Environ. Microbiol. 80, 5292–5303.
Tan, S.Z., Reisch, C.R., Prather, K.L.J., 2018. A robust CRISPR interference gene repression system in *Pseudomonas*. J. Bacteriol. 200, e00575–17.
Tao, S., Qian, Y., Wang, X., Cao, W., Ma, W., Chen, K., Ouyang, P., 2018. Regulation of ATP levels in *Escherichia coli* using CRISPR interference for enhanced pinocembrin production. Microb. Cell Factories 17, 147.
Tao, W., Lv, L., Chen, G.Q., 2017. Engineering *Halomonas* species TD01 for enhanced polyhydroxyalkanoates synthesis *via* CRISPRi. Microb. Cell Factories 16, 48.
Tarasava, K., Oh, E.J., Eckert, C.A., Gill, R.T., 2018. CRISPR-enabled tools for engineering microbial genomes and phenotypes. Biotechnol. J. 13, e1700586.
Thompson, M.G., Incha, M.R., Pearson, A.N., Schmidt, M., Sharpless, W.A., Eiben, C.B., Cruz-Morales, P., Blake-Hedges, J.M., Liu, Y., Adams, C.A., Haushalter, R.W., Krishna, R.N., Lichtner, P., Blank, L.M., Mukhopadhyay, A., Deutschbauer, A.M., Shih, P.M., Keasling, J.D., 2020. Fatty acid and alcohol metabolism in *Pseudomonas putida*: functional analysis using random barcode transposon sequencing. Appl. Environ. Microbiol. 86, e01665–20.
Tokic, M., Hatzimanikatis, V., Miskovic, L., 2020. Large-scale kinetic metabolic models of *Pseudomonas putida* KT2440 for consistent design of metabolic engineering strategies. Biotechnol. Biofuels 13, 33.
Tokuyama, K., Toya, Y., Matsuda, F., Cress, B.F., Koffas, M.A.G., Shimizu, H., 2019. Magnesium starvation improves production of malonyl-CoA-derived metabolites in *Escherichia coli*. Metab. Eng. 52, 215–223.
Tovilla-Coutiño, D.B., Momany, C., Eiteman, M.A., 2020. Engineered citrate synthase alters acetate accumulation in *Escherichia coli*. Metab. Eng. 61, 171–180.
Tran, L.M., Rizk, M.L., Liao, J.C., 2008. Ensemble modeling of metabolic networks. Biophys. J. 95, 5606–5617.
Udaondo, Z., Molina, L., Segura, A., Duque, E., Ramos, J.L., 2016. Analysis of the core genome and pangenome of *Pseudomonas putida*. Environ. Microbiol. 18, 3268–3283.
Volke, D.C., Nikel, P.I., 2018. Getting bacteria in shape: synthetic morphology approaches for the design of efficient microbial cell factories. Adv. Biosyst. 2, 1800111.
Volke, D.C., Calero, P., Nikel, P.I., 2020a. Pseudomonas putida. Trends Microbiol. 28, 512–513.
Volke, D.C., Friis, L., Wirth, N.T., Turlin, J., Nikel, P.I., 2020b. Synthetic control of plasmid replication enables target- and self-curing of vectors and expedites genome engineering of *Pseudomonas putida*. Metab. Eng. Commun. 10, e00126.
Volke, D.C., Turlin, J., Mol, V., Nikel, P.I., 2020c. Physical decoupling of XylS/*Pm* regulatory elements and conditional proteolysis enable precise control of gene expression in *Pseudomonas putida*. Microb. Biotechnol. 13, 222–232.
Volke, D.C., Olavarría, K., Nikel, P.I., 2021. Cofactor specificity of glucose-6-phosphate dehydrogenase isozymes in *Pseudomonas putida* reveals a general principle underlying glycolytic strategies in bacteria. mSystems 6, e00014–21.
Volkova, S., Matos, M.R.A., Mattanovich, M., Marín de Mas, I., 2020. Metabolic modelling as a framework for metabolomics data integration and analysis. Metabolites 10, 303.
Weimer, A., Kohlstedt, M., Volke, D.C., Nikel, P.I., Wittmann, C., 2020. Industrial biotechnology of *Pseudomonas putida*: advances and prospects. Appl. Microbiol. Biotechnol. 104, 7745–7766.
Wirth, N.T., Kozaeva, E., Nikel, P.I., 2020. Accelerated genome engineering of *Pseudomonas putida* by I-*Sce*I–mediated recombination and CRISPR-Cas9 counterselection. Microb. Biotechnol. 13, 233–249.
Woolston, B.M., Emerson, D.F., Currie, D.H., Stephanopoulos, G., 2018. Rediverting carbon flux in *Clostridium ljungdahlii* using CRISPR interference (CRISPRi). Metab. Eng. 48, 243–253.
Worsey, M.J., Williams, P.A., 1975. Metabolism of toluene and xylenes by *Pseudomonas putida* (*arvilla*) mt-2: evidence for a new function of the TOL plasmid. J. Bacteriol. 124, 7–13.
Xu, X., Qi, L.S., 2019. A CRISPR-dCas toolbox for genetic engineering and synthetic biology. J. Mol. Biol. 431, 34–47.
Young, R., Haines, M., Storch, M., Freemont, P.S., 2021. Combinatorial metabolic pathway assembly approaches and toolkits for modular assembly. Metab. Eng. 63, 81–101.
Zhang, R., Xu, W., Shao, S., Wang, Q., 2021. Gene silencing through CRISPR interference in bacteria: current advances and future prospects. Front. Microbiol. 12, 635227.
Zhang, X., Lin, Y., Wu, Q., Wang, Y., Chen, G.Q., 2020. Synthetic biology and genome-editing tools for improving PHA metabolic engineering. Trends Biotechnol. 38, 689–700.
Zhang, X.C., Guo, Y., Liu, X., Chen, X.G., Wu, Q., Chen, G.Q., 2018. Engineering cell wall synthesis mechanism for enhanced PHB accumulation in *E. coli*. Metab. Eng. 45, 32–42.
Zhao, D., Zhu, X., Zhou, H., Sun, N., Wang, T., Bi, C., Zhang, X., 2021. CRISPR-based metabolic pathway engineering. Metab. Eng. 63, 148–159.
Zhou, S., Lama, S., Jiang, J., Sankaranarayanan, M., Park, S., 2020. Use of acetate for the production of 3-hydroxypropionic acid by metabolically-engineered *Pseudomonas denitrificans*. Bioresour. Technol. 307, 123194.